


# Toll-like receptor 2 deficiency hyperactivates the FoxO1 transcription factor and induces aging-associated cardiac dysfunction in mice

Received for publication, January 12, 2018, and in revised form, June 9, 2018. Published, Papers in Press, June 21, 2018, DOI 10.1074/jbc.RA118.001880

Kondapalli Mrudula Spurthi<sup>‡1</sup>, Mohsen Sarikhani<sup>‡2</sup>, Sneha Mishra<sup>‡2</sup>, Perumal Arumugam Desingu<sup>‡2,3</sup>, Shikha Yadav<sup>§</sup>, Swathi Rao<sup>‡</sup>, Sangeeta Maity<sup>‡</sup>, Ankit Kumar Tamta<sup>‡</sup>, Shweta Kumar<sup>‡</sup>, Shamik Majumdar<sup>§</sup>, Aditi Jain<sup>¶</sup>, Aishwarya Raghuraman<sup>‡</sup>, Danish Khan<sup>‡</sup>, Ishwar Singh<sup>‡</sup>, Rosa J. Samuel<sup>||</sup>, Subbaraya G. Ramachandra<sup>||</sup>,  Dipankar Nandi<sup>§</sup>, and Nagalingam R. Sundaresan<sup>‡4</sup>

From the <sup>‡</sup>Department of Microbiology and Cell Biology, Indian Institute of Science, Bengaluru, Karnataka 560012, India, the <sup>§</sup>Department of Biochemistry, Indian Institute of Science, Bengaluru, Karnataka 560012, India, the <sup>¶</sup>Centre for Biosystems Science and Engineering, Indian Institute of Science, Bengaluru, Karnataka 560012, India, and the <sup>||</sup>Central Animal Facility, Indian Institute of Science, Bengaluru, Karnataka 560012, India

Edited by Alex Tokor

Toll-like receptors (TLRs) are a family of pattern-recognition receptors involved in innate immunity. Previous studies have shown that TLR2 inhibition protects the heart from acute stress, including myocardial infarction and doxorubicin-induced cardiotoxicity in animal models. However, the role of TLR2 in the development of aging-associated heart failure is not known. In this work, we studied aging-associated changes in structure and function of TLR2-deficient mice hearts. Whereas young TLR2-KO mice did not develop marked cardiac dysfunction, 8- and 12-month-old TLR2-KO mice exhibited spontaneous adverse cardiac remodeling and cardiac dysfunction in an age-dependent manner. The hearts of the 8-month-old TLR2-KO mice had increased fibrosis, cell death, and reactivation of fetal genes. Moreover, TLR2-KO hearts displayed reduced infiltration by macrophages, increased numbers of myofibroblasts and atrophic cardiomyocytes, and higher levels of the atrophy-related ubiquitin ligases MuRF-1 and atrogin-1. Mechanistically, TLR2 deficiency impaired the PI3K/Akt signaling pathway, leading to hyperactivation of the transcription factor Forkhead box protein O1 (FoxO1) and, in turn, to elevated expression of FoxO target genes involved in the regulation of muscle wasting and cell death. AS1842856-mediated chemical inhibition of FoxO1 reduced the expression of the atrophy-related ubiquitin ligases and significantly reversed the adverse cardiac remodel-

ing while improving the contractile functions in the TLR2-KO mice. Interestingly, TLR2 levels decreased in hearts of older mice, and the activation of TLR1/2 signaling improved cardiac functions in these mice. These findings suggest that TLR2 signaling is essential for protecting the heart against aging-associated adverse remodeling and contractile dysfunction in mice.

The mammalian heart responds to injury caused by infections, myocardial infarction, atherosclerosis, and pressure overload by activating both the innate and the adaptive arms of immunity (1). In response to cardiac injury, immunological responses are activated to protect cardiomyocytes and promote tissue repair (1). It is worth mentioning that inflammation is associated with several forms of clinical heart failure (2). Importantly, inflammation drives left ventricular remodeling and cardiac dysfunction in the heart (3, 4). Specifically, proinflammatory cytokines, released by the inflammatory stimuli, are sufficient to induce cardiac dysfunction in experimental animals (4). Therefore, several multicenter clinical trials were initiated in the last decade to treat heart failure by minimizing inflammation in patients with moderate to advanced heart failure, by targeting tumor necrosis factor (TNF),<sup>5</sup> a key inflammatory mediator. However, the targeted anti-TNF approaches did not reduce heart failure and, instead, led to worsening of heart functions, thus causing death in patients (5, 6). Collectively, these studies provided evidence that inflammation might play a

This work was supported by Grant EMR/2014/000065 from the Department of Science and Technology (DST) Extramural Research, Grants BRB/10/1294/2014 and MED/30/1454/2014 from the Department of Biotechnology Extramural Research, and Grant 37(1646)/15/EMR-II from the Council for Scientific and Industrial Research Extramural Research. The authors declare that they have no conflicts of interest with the contents of this article.

This article contains Fig. S1.

<sup>1</sup> Supported by a Science and Engineering Research Board (SERB) National Post-doctoral Fellowship (N-PDF).

<sup>2</sup> These authors contributed equally to this work.

<sup>3</sup> A DST INSPIRE faculty fellow.

<sup>4</sup> Supported by a Ramalingaswami Re-entry Fellowship and an Innovative Young Biotechnologist Award (IYBA) from the Department of Biotechnology, Government of India. To whom correspondence should be addressed: SB-02, Dept. of Microbiology and Cell Biology, Division of Biological Sciences, Indian Inst. of Science, Bengaluru, Karnataka 560012, India. Tel.: 91-80-2293-2068; Fax: 91-80-2360-2697; E-mail: rsundaresan@iisc.ac.in.

<sup>5</sup> The abbreviations used are: TNF, tumor necrosis factor; TLR, Toll-like receptor; PAMP, pathogen-associated molecular pattern; DAMP, damage-associated molecular pattern; HW/BW, heart weight to body weight; HW/TL, heart weight to tibia length; LVID, left ventricular internal diameter; qPCR, quantitative PCR; ANP, atrial natriuretic peptide; BNP, brain natriuretic peptide; MHC, myosin heavy chain; TUNEL, terminal deoxynucleotidyl-transferase-mediated dUTP nick end labeling; WGA, wheat germ agglutinin; MCP-1, monocyte chemoattractant protein 1; ICAM-1, intercellular adhesion molecule 1; VCAM-1, vascular cell adhesion molecule 1; GADPH, glyceraldehyde-3-phosphate dehydrogenase; HRP, horseradish peroxidase; SSC-A, side scatter area; ANOVA, analysis of variance; BAX, BCL2-associated X; AIF, apoptosis-inducing factor; TRAIL, TNF-related apoptosis-inducing ligand; PE, phycoerythrin.

protective role in the heart and that blocking inflammatory responses may be detrimental to failing hearts.

Toll-like receptors (TLR) are pattern-recognition receptor proteins capable of recognizing pathogen-associated molecular patterns (PAMP) and damage-associated molecular patterns (DAMP), such as viral proteins, lipopolysaccharides, peptidoglycan, and RNA and DNA molecules (7, 8). Following the activation of TLRs, immune cells produce several inflammatory molecules such as TNF $\alpha$ , IL1 $\beta$ , and IL6, etc. (9). Apart from PAMPs, the activation of TLRs also depends on the presence of DAMPs, which are released by the injured cells. DAMP recognition is involved in the sensing of an ongoing infection to recruit more cells as well as to initiate the repair of damaged tissue. There are endogenous TLR ligands derived from the host tissue or cells, which may either be components of the cells or induced gene products under specific conditions (10). The majority of these ligands are components of the extracellular matrix, including fibronectin, biglycan, heparan sulfate, fibrinogen, hyaluronan breakdown fragments, and oligosaccharides of hyaluronan (11). Apart from extracellular matrix components, biglycan, endoplasmic reticulum stress proteins, HMGB1, HSP60, HSP70, human cardiac myosin, hyaluronan, and monosodium urate crystals are endogenous ligands for TLR2. Importantly, these endogenous TLR ligands play a key role in the activation of TLRs during the cardiac injury (11).

Although TLRs are generally expressed in immune cells, TLR2, a member of the TLR family, is expressed in nonimmune cells of the heart including cardiomyocytes, fibroblasts, and vascular endothelial cells (12). Interestingly, the expression of TLR2 is enhanced in several forms of heart failure (13–15). Studies have shown that TLR2 deficiency attenuates myocardial inflammation, reduces infarct size, and preserves ventricular function after ischemic injury in animal models (16). Moreover, TLR2 deficiency preserves the cardiac structure and ventricular function after acute myocardial infarction (17). In experimental mice models, TLR2 deficiency attenuated *Staphylococcus aureus*- or doxorubicin-induced cardiac dysfunction (18, 19). Along similar lines, TLR2 deficiency reduces the severity of atherosclerosis in low-density lipoprotein receptor-deficient mice (20). In contrast to these studies suggesting a detrimental role for TLR2 signaling in heart, a few recent reports suggest that TLR2 deficiency exacerbates cardiac hypertrophy and remodeling after transverse aortic constriction in mice (12, 21). Notably, TLR2 deficiency causes mature-onset obesity in mice and increases the susceptibility to high-fat diet-induced weight gain. TLR2-deficient mice weighed almost 30% more than their WT counterparts at 12 months of age (22), suggesting that TLR2 deficiency increases susceptibility to metabolic diseases in an aging-dependent manner. Along similar lines, TLR2-deficient mice develop severe colitis, which is also associated with aging (23). It is worth mentioning that TLR signaling is impaired during aging (24). Overall, these studies suggest that an aging-related decline in TLR2 functions might increase susceptibility to aging-related diseases such as obesity and colitis. However, there is no information available for the role of TLR2 in regulating cardiac aging in mice.

One of the major signaling pathways activated downstream of TLR2 is PI3K/Akt signaling (25–27). TLR2 is reported to

contain a PI3K-binding motif (YXXM) in its cytoplasmic domain, which is responsible for binding TLR2 to the p85 subunit of PI3K (25). Interestingly, activation of the PI3K/Akt signaling prevents cardiomyocyte apoptosis as well as ischemia/reperfusion injury in the myocardium (27, 28). The activated Akt phosphorylates and inhibits FoxO transcription factors, well-known downstream targets of Akt, thus contributing to cell survival, cell growth, and proliferation (29). In human failing hearts the activity of Akt decreases, but the activity of FoxO and atrogen-1, its target, increases (30). Three members of the FoxO subfamily, FoxO1, FoxO3, and FoxO4, are essential for maintaining cardiac homeostasis. FoxO transcription factors bind to a conserved DNA-binding sequence, TTGTTTAC, and work with several transcription factors such as  $\beta$ -catenin, Notch, Smad, and PGC-1 $\alpha$  as coactivators (29). The FoxO transcription factors are highly expressed in mice models for cardiac failure (31) and in the end-stage human failing heart (32). Importantly, overexpression of FoxO is sufficient to induce adverse remodeling and contractile dysfunction in mice (31). The activation of FoxO induces cell death through increased transcription of its target genes, including TRAIL, Bim, and FasL. In addition, FoxO activation induces cell cycle arrest via transcription of p27<sup>kip1</sup>, p21<sup>cip1</sup>, and GADD45A. Interestingly, FoxO activation transcriptionally up-regulates the expression of the muscle-specific ubiquitin ligases atrogen-1/MAFbx and MuRF1 to induce muscle wasting in heart (29).

In this work, we investigated the aging-associated changes in the structure and function of TLR2-deficient mice hearts. Interestingly, our results suggest that TLR2-deficient mice develop aging-related cardiac dysfunction because of impaired Akt signaling and subsequent hyperactivation of FoxO transcription factors in the heart. Our results also indicate that the activation of TLR signaling improved contractile functions in aged mice.

## Results

### TLR2-deficient mice develop spontaneous gender-independent accelerated cardiac aging and dysfunction

To study whether the loss of TLR2 increases susceptibility to aging-associated cardiac remodeling and dysfunction, we analyzed the cardiac functions of TLR2-deficient (TLR2-KO) male mice at 2, 8, and 12 months of age by transthoracic echocardiography. TLR2-KO mice lack TLR2 in all cell types found in the mice. At 2 months of age, TLR2-KO male mice had increased body weight but did not exhibit any evident changes in heart weight to body weight (HW/BW) ratio and heart weight to tibia length (HW/TL) ratio, which are indicators of cardiac hypertrophy (Fig. 1, A–C). However, our results show a mild reduction in the left ventricular posterior wall thickness, fractional shortening, and an increase in the left ventricular internal diameter (LVID) in 2-month-old TLR2-KO male mice when compared with age-matched controls (Fig. 1, D–F). When we analyzed the body weight, cardiac structure, and functions of 8- and 12-month-old TLR2-KO male mice, we found significant increases in body weight, HW/BW ratio, HW/TL ratio, and LVID and reduced ventricular posterior wall thickness, as compared with age-matched control male mice

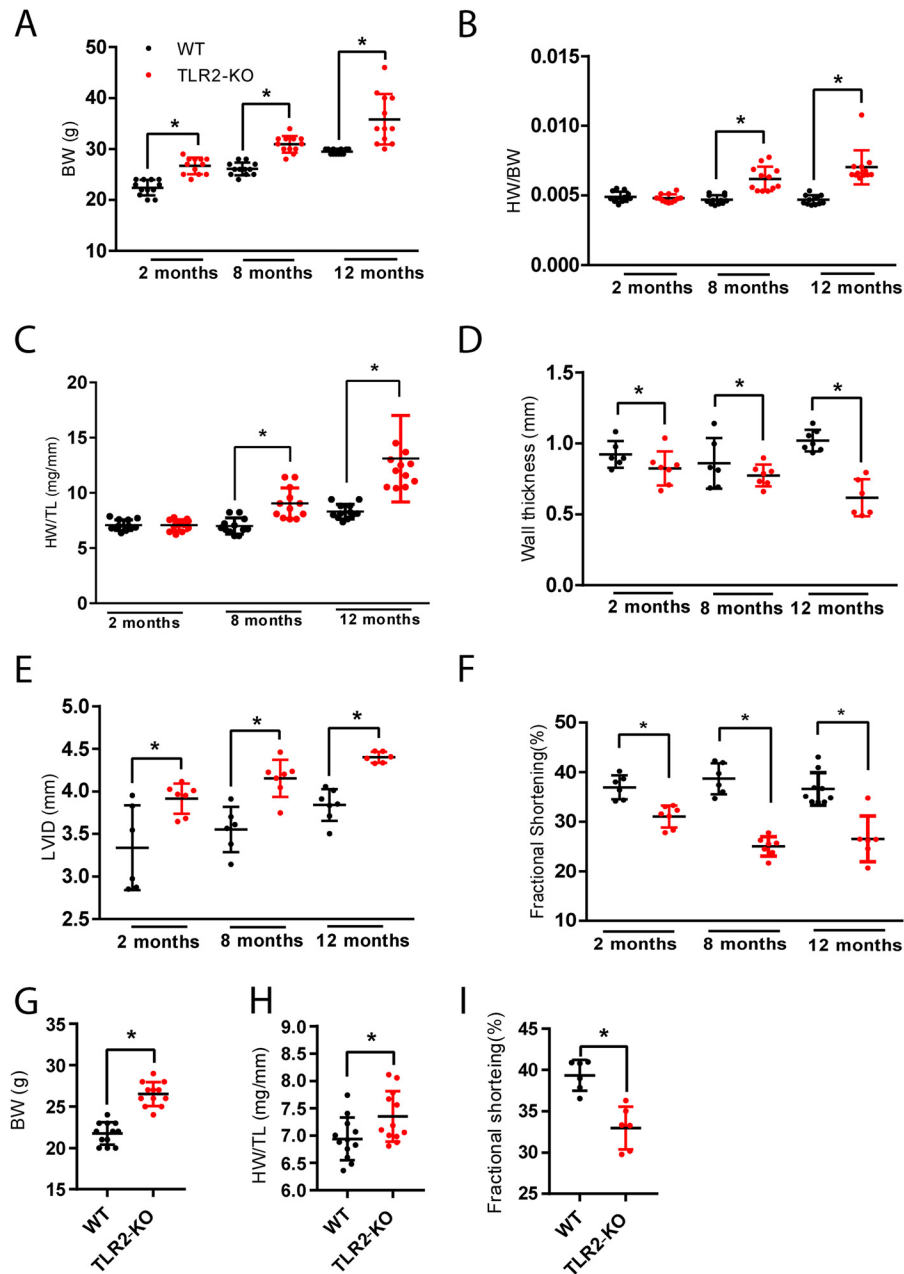


**Figure 1. TLR2 deficiency induces cardiac remodeling and dysfunction.** A, graph representing body weight (g) of WT and TLR2-KO male mice of different age groups (2, 8, and 12 months).  $n = 12$  mice/group. Data are presented as mean  $\pm$  S.D.; \*,  $p < 0.05$ . One-way ANOVA was used to calculate the  $p$  values. B, graph showing HW/BW ratio of WT and TLR2-KO male mice of different age groups (2, 8, and 12 months).  $n = 12$  mice/group. Data are presented as mean  $\pm$  S.D.; \*,  $p < 0.05$ . One-way ANOVA was used to calculate the  $p$  values. C, graph depicting HW/TL (mg/mm) ratio of WT and TLR2-KO male mice of different age groups (2, 8, and 12 months).  $n = 12$  mice/group. Data are presented as mean  $\pm$  S.D.; \*,  $p < 0.05$ . One-way ANOVA was used to calculate the  $p$  values. D, graph representing left ventricular posterior wall thickness (mm) at diastole of WT and TLR2-KO male mice of different age groups (2, 8, and 12 months).  $n = 6-7$  mice/group. Data are presented as mean  $\pm$  S.D.; \*,  $p < 0.05$ . One-way ANOVA was used to calculate the  $p$  values. E, graph showing left ventricular internal diameter (mm) during diastole of WT and TLR2-KO male mice of different age groups (2, 8, and 12 months).  $n = 6-7$  mice/group. Data are presented as mean  $\pm$  S.D.; \*,  $p < 0.05$ . One-way ANOVA was used to calculate the  $p$  values. F, graph showing the contractile functions of heart as represented by fractional shortening (%) of WT and TLR2-KO male mice of different age groups (2, 8, and 12 months).  $n = 6-9$  mice/group. Data are presented as mean  $\pm$  S.D.; \*,  $p < 0.05$ . One-way ANOVA was used to calculate the  $p$  values. G, graph representing body weight (g) of 8-month-old WT and TLR2-KO female mice.  $n = 12$  mice/group. Data are presented as mean  $\pm$  S.D.; \*,  $p < 0.05$ . Student's  $t$  test was used to calculate the  $p$  value. H, graph depicting HW/TL (mg/mm) ratio of 8-month-old WT and TLR2-KO female mice.  $n = 12$  mice/group. Data are presented as mean  $\pm$  S.D.; \*,  $p < 0.05$ . Student's  $t$  test was used to calculate the  $p$  value. I, graph showing the contractile functions of heart as represented by fractional shortening (%) of 8-month-old WT and TLR2-KO female mice.  $n = 6$  mice/group. Data are presented as mean  $\pm$  S.D.; \*,  $p < 0.05$ . Student's  $t$  test was used to calculate the  $p$  value.

(Fig. 1, A–E). These results suggest that TLR2 deficiency induces adverse cardiac remodeling and, specifically TLR2-KO mice hearts exhibit spontaneous aging-related heart failure. Interestingly, TLR2 deficiency caused almost a 30% reduction in fractional shortening in both 8- and 12-month-old male mice

(Fig. 1F), suggesting that chronic TLR2 deficiency causes contractile dysfunction in male mouse hearts. These overall changes closely resemble the cardiac structure and function of aged mice, which exhibit increased left ventricular dimension, decreased wall thickness, and decreased fractional shortening



## TLR2 deficiency induces aging-related heart failure

(33, 34). To check whether the development of adverse remodeling and cardiac dysfunction is gender-dependent, we analyzed the cardiac structure and function of 8-month-old WT and TLR2-KO female mice. Our results revealed that female TLR2-KO mice develop adverse remodeling and contractile dysfunction, as observed in TLR2-KO male mice (Fig. 1, *G–I*). These findings collectively suggest that TLR2 deficiency induces spontaneous cardiac remodeling and dysfunction in an age-dependent and gender-independent manner. Therefore, we performed all further experiments in 8-month-old TLR2-deficient male mice, unless specified.

### TLR2-deficient mice hearts exhibit increased fibrosis and express fetal genes

Because hearts exhibiting aging-related failure show a reactivation of fetal genes (35), we quantified the expression of fetal genes in TLR2-KO mice hearts by qPCR analysis. Our results indicated significantly increased expression of the cardiac fetal genes for atrial natriuretic peptide (ANP), brain natriuretic peptide (BNP), and myosin heavy chain,  $\beta$  isoform ( $\beta$ -MHC) in 8-month-old TLR2-KO hearts (Fig. 2*A*). On the other hand, the expression of myosin heavy chain,  $\alpha$  isoform ( $\alpha$ -MHC) was markedly lower in these TLR2-KO hearts (Fig. 2*A*). Further Western blot analysis for ANP also showed significantly higher expression levels in TLR2-KO mice heart samples as compared with the WT controls at 8 months of age (Fig. 2*B*). These findings revealed that TLR2 deficiency reactivates fetal genes, one of the markers of aging hearts. The aging heart is characterized by structural and morphological alterations, and one of those key event is loss of elasticity by increased fibrosis (36). Our histological analysis revealed no difference in the extent of fibrosis between 2-month-old WT and TLR2-KO mice (Fig. 2, *C and E*). However, analysis of 8-month-old TLR2-KO mice heart sections revealed a significant increase in interstitial fibrosis in the ventricle (Fig. 2*D*, row *I*), interstitial fibrosis in the atrium (Fig. 2*D*, row *II*), replacement fibrosis in the ventricle (Fig. 2*D*, row *III*), mitral valve fibrosis (Fig. 2*D*, row *IV*), and perivascular fibrosis, both in a cross-section (Fig. 2*D*, row *V*) and in a longitudinal section (Fig. 2*D*, row *VI*). Quantification suggested an increase in fibrosis in the 8-month-old TLR2-KO mice heart samples (Fig. 2*E*). Interestingly, our findings of increased mitral valve fibrosis suggest that TLR2-KO mice develops accelerated cardiac aging (37). To check whether this cardiac dysfunction is associated with trans-differentiation of fibroblasts to myofibroblasts, we performed immunohistochemistry using specific antibody against periostin, a marker for myofibroblast. We observed a markedly higher number of myofibroblasts in TLR2 knockout mice hearts as compared with the WT mice hearts (Fig. 2*F*). Consistent with the histology analysis, we also found changes in the expression of fibrotic markers such as fibronectin-1 (Fn1) and  $\alpha$ -smooth muscle actin ( $\alpha$ -SMA), and periostin in TLR2-KO heart lysates (Fig. 2, *G and H*). These findings suggest that deficiency of TLR2 might activate fetal gene program and induce fibrosis, which could be the reason for the adverse remodeling and contractile dysfunction in the heart.

### TLR2-deficient hearts show increased cell death

Cardiomyocyte cell death, either apoptotic or necrotic in nature, constitutes a key determinant of the aging process in the heart (38). TUNEL assay results revealed an increased number of apoptotic nuclei in the TLR2-KO mice hearts as compared with control mice at 8 months but not at 2 months of age (Fig. 3, *A and B*). We performed Western blot analysis for cell death markers. Our results suggested that TLR2-KO hearts exhibit higher levels of cleaved PARP-1 and cleaved caspase-3, both of which are well-known indicators of cell death (39) (Fig. 3*C*). Interestingly, we also found an increase in the levels of total PARP-1 in TLR2-KO mice. This is in accordance with previous studies that show up-regulated expression of PARP-1 in failing human hearts (40). Because TUNEL and Western blot assay results showed increased cell death in TLR2-deficient hearts, we checked whether TLR2-KO hearts would show muscle wasting accompanied by atrophic cardiomyocytes (33). We measured the cardiomyocyte cross-sectional area by wheat germ agglutinin (WGA) staining to identify the proportion of atrophic cells in TLR2-KO heart sections. wheat germ agglutinin-Alexa Fluor 594 staining was used to visualize cardiomyocyte cell membranes, where atrophic cardiomyocytes exhibit smaller cell area (41). About 4% of the cells in control hearts showed atrophic cardiomyocytes, whereas TLR2-KO heart sections exhibited a significantly higher number of atrophic cardiomyocytes (27%) (Fig. 3, *D and E*). To further test for muscle wasting, we measured the expression levels of muscle-specific ubiquitin ligases, atrogin-1 and MuRF-1, which are well-established markers for muscle wasting. We found increased mRNA levels of both atrogin-1 and MuRF-1 in TLR2-KO hearts (Fig. 3*F*). To further validate these findings, we performed Western blot analysis for the atrophic markers atrogin-1, MuRF-1, and ubiquitin. Our results revealed increased levels of atrogin-1, MuRF-1, and total ubiquitin in TLR2-KO hearts (Fig. 3, *G and H*). These findings indicate that TLR2 deficiency induces cell death and muscle wasting in an aging-dependent manner and could be the major contributor for remodeling and dysfunction in the heart.

### TLR2-deficient hearts harbor reduced residual macrophages and neutrophils

An age-dependent decline in the number of macrophages has been observed in aging hearts (34, 42). Therefore, we tested whether TLR2-KO hearts showed any changes in the population of macrophages in the heart. We performed histological analysis to localize the macrophages in control and TLR2-KO mice hearts. We observed a reduction in the number of macrophages in the myocardium of 8-month-old TLR2-KO mice as compared with the WT mice (Fig. 4*A*). In accordance with previous studies (13), flow cytometric analysis of adult mice hearts showed a decrease in the number of macrophages in TLR2-KO heart samples as compared with the control heart samples (Fig. 4, *B and C*). These findings are also consistent with the reports showing down-regulation of immune response genes (42). Interestingly, we found a lesser number of neutrophils in TLR2-KO hearts (Fig. 4, *B and D*), suggesting that TLR2 deficiency impairs the resident macrophages population without

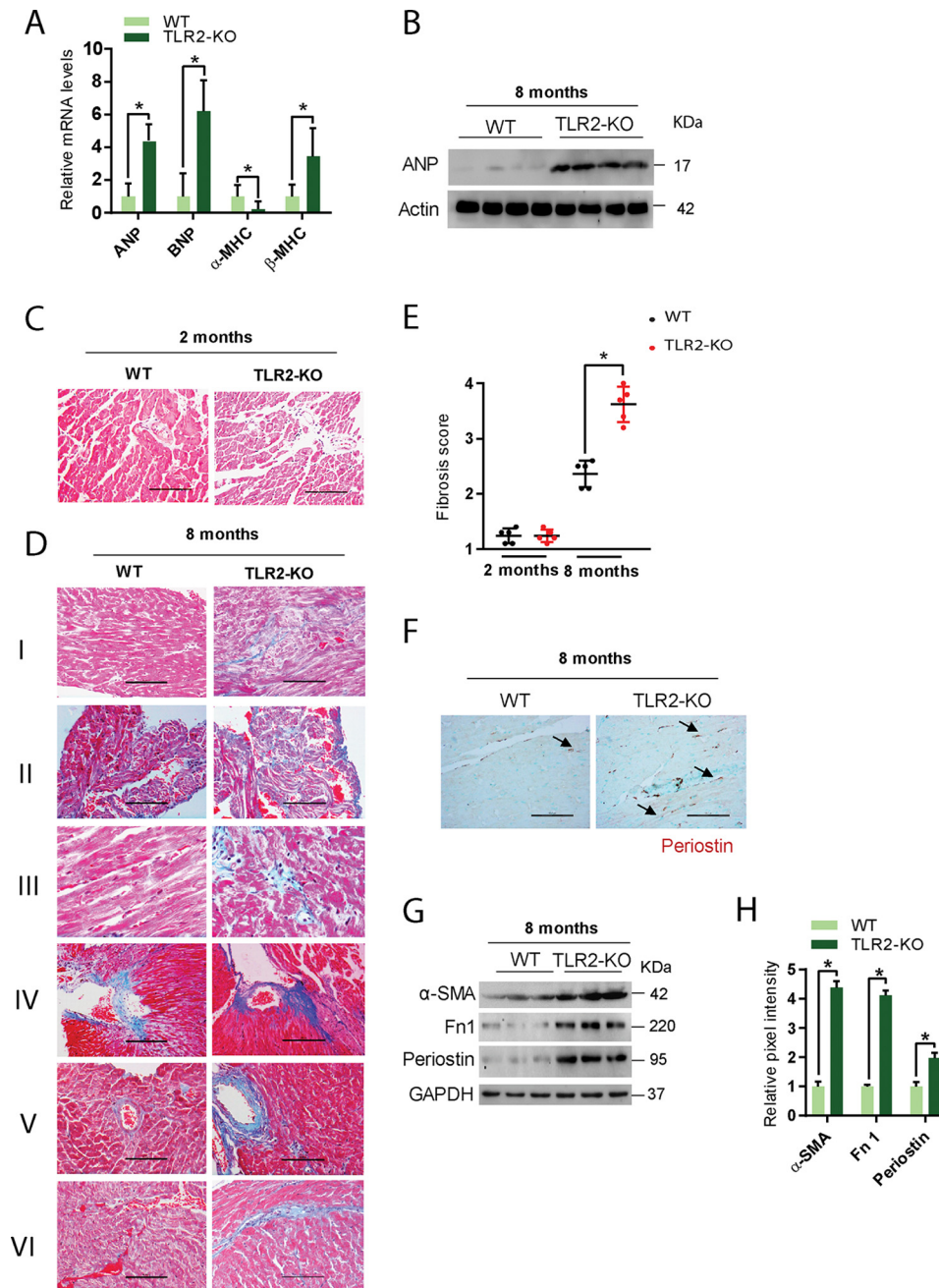


**Figure 2. TLR2 deficiency reactivates fetal gene program and induces cardiac fibrosis.** *A*, qPCR analysis of ANP, BNP, and MHC- $\alpha$  and - $\beta$  isoforms in hearts of 8-month-old WT and TLR2-KO male mice. Actin was used as the housekeeping gene.  $n = 6-13$  mice/group. Data are presented as mean  $\pm$  S.D.; \*,  $p < 0.05$ . Student's  $t$  test was used to calculate the  $p$  values. *B*, representative Western blot analysis of ANP and GAPDH in heart lysates of 8-month-old WT and TLR2-KO male mice.  $n = 8$  mice/group. Our analysis showed that one of eight WT mice displayed ANP expression in the heart. However, seven of eight TLR2-KO mice showed ANP expression in the heart lysates. *C*, heart sections of 2-month-old WT and TLR2-KO male mice stained with Masson's trichrome stain.  $n = 5$  mice/group. Scale bar = 100  $\mu$ m. Results show no obvious fibrosis in these mice. *D*, heart sections of 8-month-old WT and TLR2-KO male mice stained with Masson's trichrome stain showing cardiac fibrosis. Blue color indicates the presence of collagen. *I*, interstitial fibrosis in ventricle; *II*, interstitial fibrosis in atrium; *III*, replacement fibrosis; *IV*, mitral valve fibrosis; *V*, perivascular fibrosis in cross-section; and *VI*, longitudinal section in TLR2-KO hearts.  $n = 5$  mice/group. Scale bar = 100  $\mu$ m. *E*, graph showing fibrosis scored in a blinded fashion in heart sections of 8-month-old WT and TLR2-KO male mice stained with Masson's trichrome stain. The protocol for scoring fibrosis is described under "Experimental procedures."  $n = 5$  mice/group. Data are presented as mean  $\pm$  S.D.; \*,  $p < 0.05$ . One-way ANOVA was used to calculate the  $p$  values. *F*, representative confocal images stained for periostin, a myofibroblast marker in sections of WT and TLR2-KO male mice hearts at 8 months of age. Scale bar = 100  $\mu$ m. TLR2-KO mice hearts show more periostin-positive cells, which are stained brown and marked by black arrows.  $n = 5$  mice/group. *G*, representative Western blot images showing the expression of markers of fibrosis, i.e.  $\alpha$ -smooth muscle actin ( $\alpha$ -SMA), Fn1 and periostin in 8-month-old WT and TLR2-KO male mice heart samples ( $n = 6$  mice/group). *H*, graph showing the quantification of the protein levels of  $\alpha$ -smooth muscle actin, fibronectin-1, and periostin, which are markers of fibrosis in 8-month-old WT and TLR2-KO male mice heart samples.  $n = 6$  mice/group. Data are presented as mean  $\pm$  S.D.; \*,  $p < 0.05$ . Student's  $t$  test was used to calculate the  $p$  values.

increasing the neutrophils in the heart. Next, using ELISA we tested whether TLR2 deficiency modulated the serum cytokine profile. Our results suggested that TLR2 deficiency does not

influence the circulating cytokine levels (Fig. 4E). We also assessed the cytokine mRNA levels in the heart tissues of TLR2-KO mice and found no significant changes (Fig. 4F).

## TLR2 deficiency induces aging-related heart failure

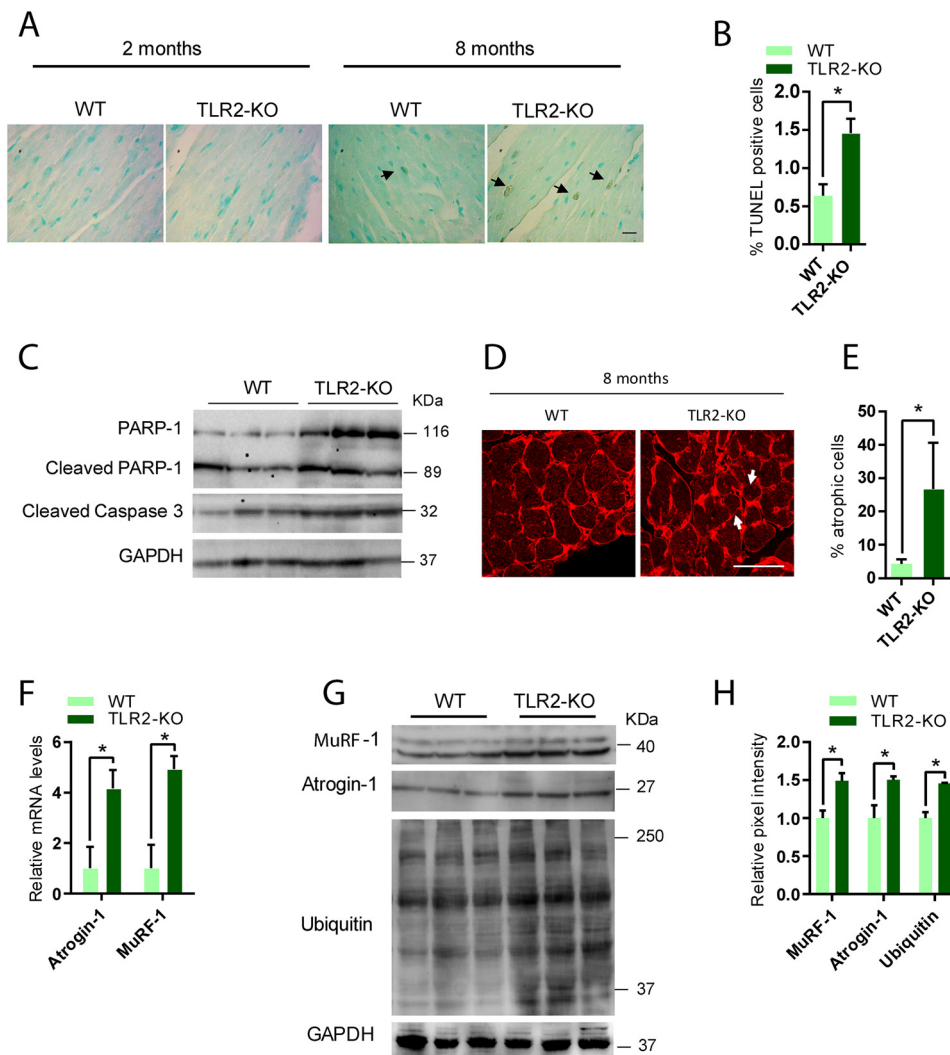


**Figure 3. TLR2 deficiency promotes cardiac cell death.** A, representative images of TUNEL assay showing cell death in sections of WT and TLR2-KO male mice hearts at 2 and 8 months of age. Brown nuclei indicate the TUNEL-positive cells, which are marked by black arrows.  $n = 5$  mice/group. Scale bar = 20  $\mu\text{m}$ . B, quantification of percentage of TUNEL-positive cells in sections of WT and TLR2-KO male mice hearts at 8 months of age.  $n = 5$  mice/group. Data are presented as mean  $\pm$  S.D.; \*,  $p < 0.05$ . Student's  $t$  test was used to calculate the  $p$  value. C, representative Western blot images showing the expression of cell death markers, cleaved PARP-1, and cleaved caspase-3 in heart samples of 8-month-old WT and TLR2-KO male mice. Note that anti-caspase-3 antibody detects only the cleaved version, but not the full length.  $n = 5$  mice/group. D, representative confocal images showing WGA staining in sections of WT and TLR2-KO male mice hearts at 8 months of age. WGA stains the cell boundaries.  $n = 5$  mice/group. Scale bar = 50  $\mu\text{m}$ . E, graph showing percentage of atrophic cells measured in sections of WT and TLR2-KO male mice hearts at 8 months of age by WGA staining. Cells having a cross-sectional area of  $<700 \mu\text{m}^2$  were considered atrophic. Data are presented as mean  $\pm$  S.D.; \*,  $p < 0.05$  with Student's  $t$  test used to calculate the  $p$  value.  $n = 6$  mice/group. F, qPCR analysis of atrogin-1 and MuRF-1 mRNA levels in hearts of 8-month-old WT and TLR2-KO male mice. Actin was used as the housekeeping gene.  $n = 7$ –10 mice/group. Data are presented as mean  $\pm$  S.D.; \*,  $p < 0.05$  with Student's  $t$  test used to calculate the  $p$  values. G, representative Western blot images showing expression of atrogin-1, MuRF-1, and ubiquitin in 8-month-old WT and TLR2-KO male mice heart samples.  $n = 6$  mice/group. H, quantification of protein levels of atrogin-1, MuRF-1, and ubiquitin in 8-month-old WT and TLR2-KO male mice heart samples.  $n = 6$  mice/group. Data are presented as mean  $\pm$  S.D.; \*,  $p < 0.05$  with Student's  $t$  test used to calculate the  $p$  values.

These findings collectively indicate that the reduced macrophage population found in TLR2-deficient hearts is not related to cytokines expression.

Hearts undergoing adverse remodeling show up-regulation of cell adhesion molecules ICAM-1, VCAM-1, and MCP-1 (43, 44). Moreover, previous studies have indicated an age-dependent elevation of ICAM-1 in the heart (45). Our qPCR results indicated the up-regulation of inflammatory markers ICAM-1, VCAM-1, and MCP-1 in TLR2-KO hearts (Fig. 5A). Western blot analysis suggested that TLR2-KO hearts have increased expression of ICAM-1 (Fig. 5, B and C). These findings imply that a deficiency of TLR2 impairs the number of macrophages

and neutrophils inside the heart, even though they have increased expression levels of the cell adhesion molecules.

To investigate whether any of the other members of the TLR family compensate for a deficiency of TLR2, we performed Western blot analysis for TLR1, TLR4, and TLR6 in TLR2-deficient hearts. TLR1 expression was significantly increased in the TLR2-KO mice heart as compared with the WT. TLR4 and TLR6 expression were unaltered in TLR2-KO mice heart when compared with the WT (Fig. 5, D and E). These findings revealed that the increased TLR1 levels could be compensatory but not sufficient to rescue the defect observed in TLR2-deficient hearts. We then assessed the expression of endogenous



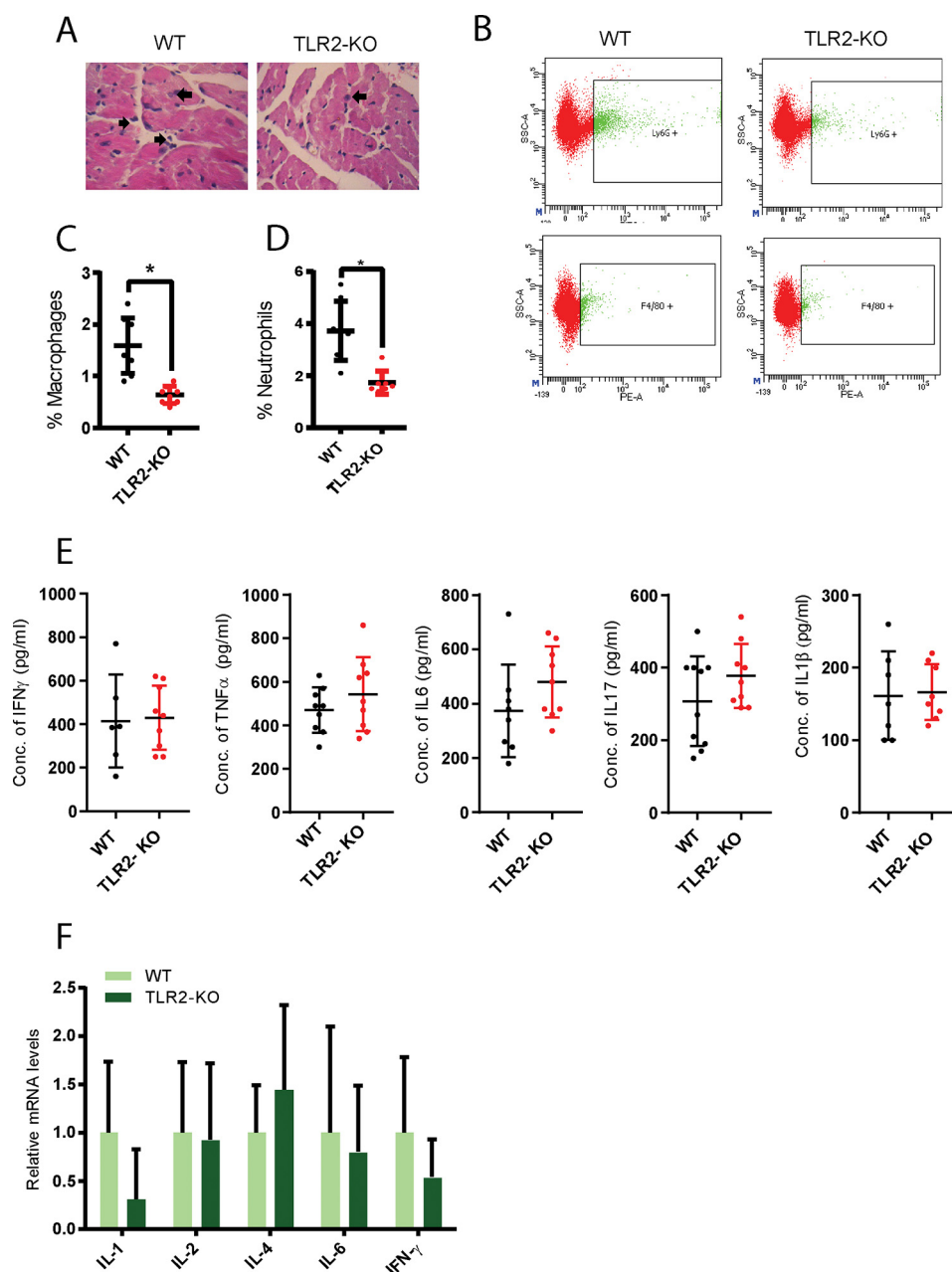


**Figure 4. TLR2 regulates macrophage infiltration to heart.** *A*, representative hematoxylin and eosin-stained images showing the macrophages in sections of WT and TLR2-KO hearts of 8-month-old male mice. *Black arrows* indicate macrophages, blindly assessed by a pathologist. *scale bar* = 20  $\mu$ m. *n* = 5 mice/group. *B*, representative scatter plots showing the Ly6G-positive neutrophils (*green*, FITC staining) and F4/80-positive macrophages (*red*, PE staining) in heart tissues of 8-month-old WT and TLR2-KO male mice assessed by flow cytometry. *n* = 7–8 mice/group. *C*, graph showing percentage of F4/80-positive macrophages in heart tissues of 8-month-old WT and TLR2-KO male mice assessed by flow cytometry. *n* = 8 mice/group. Data are presented as mean  $\pm$  S.D.; \*, *p* < 0.05 with Student's *t* test used to calculate the *p* value. *D*, graph showing percentage of neutrophils in heart tissues of 8-month-old WT and TLR2-KO male mice assessed by flow cytometry. *n* = 8 mice/group. Data are presented as mean  $\pm$  S.D.; \*, *p* < 0.05 with Student's *t* test used to calculate the *p* value. *E*, analysis of serum cytokine profile in WT and TLR2-KO mice by ELISA. *n* = 6–8 mice/group. Data are presented as mean  $\pm$  S.D.; \*, *p* < 0.05 with Student's *t* test used to calculate the *p* value. *F*, qPCR analysis of the mRNA levels of cytokines in the heart tissues of WT and TLR2-KO mice. *n* = 7–8 mice/group. Data are presented as mean  $\pm$  S.D.; \*, *p* < 0.05 with Student's *t* test used to calculate the *p* value.

TLR ligands in TLR2-KO hearts (11). Interestingly, the mRNA levels of several endogenous TLR ligands such as hsp60, hsp70, MBD2, MBD3, versican, biglycan, and Atgtr1a were up-regulated in TLR2-KO hearts (Fig. 5F). It may be because of a compensatory response to TLR2 deficiency in murine hearts.

#### TLR2 deficiency impairs Akt signaling in the heart

PI3K/Akt signaling is one of the key mediators that regulate aging-associated cardiac remodeling and muscle wasting in the

heart (46). Interestingly, TLR2 signaling has been shown to cross-talk with PI3K/Akt signaling (25–27). Therefore, we investigated the Akt signaling in young (2 months) and aged (8 months) TLR2-KO heart lysates by Western blotting. Interestingly, we found markedly lower phosphorylation of Akt at Ser-473 and its well-characterized substrates, GSK3 $\beta$  and FoxO1, and increased levels of FoxO1 (Fig. 6, *A* and *B*) in both age groups. Previous studies have demonstrated that Akt phosphorylates and inactivates FoxO by promoting its nuclear exclusion

## TLR2 deficiency induces aging-related heart failure

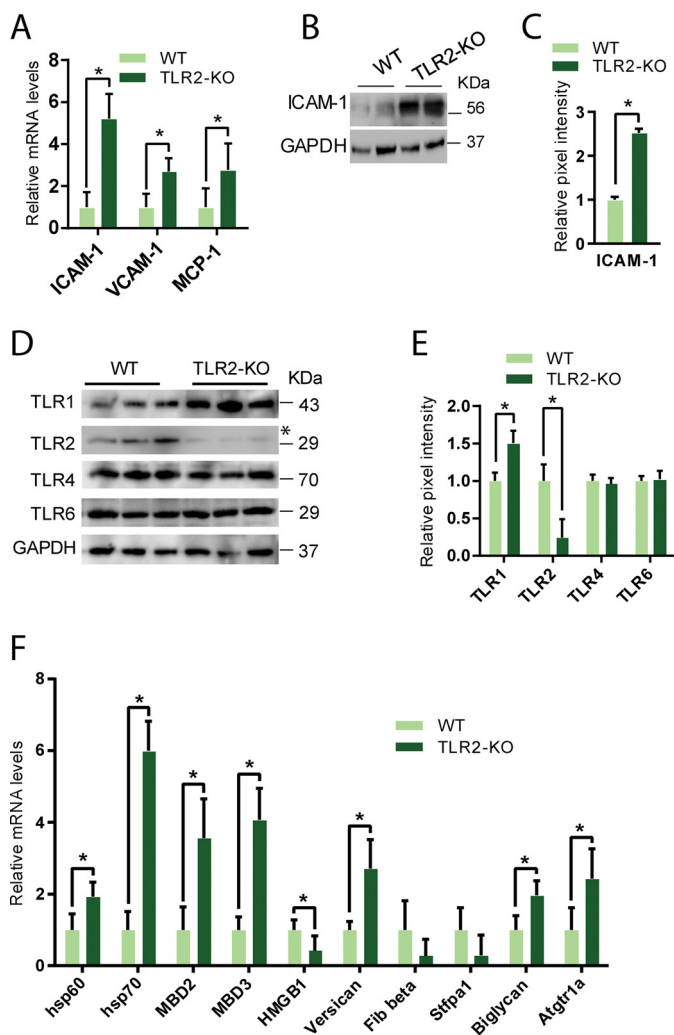


**Figure 5. TLR2 deficiency increases the expression of cell adhesion molecules in heart.** A, qPCR analysis of the mRNA levels of cell adhesion molecules, ICAM-1, VCAM-1, and MCP-1 in hearts of 8-month-old WT and TLR2-KO male mice. Actin was used as the housekeeping gene.  $n = 7-10$  mice/group. Data are presented as mean  $\pm$  S.D.; \*,  $p < 0.05$  with Student's  $t$  test used to calculate the  $p$  values. B, representative Western blot images showing the expression of ICAM-1 in heart samples of 8-month-old WT and TLR2-KO male mice.  $n = 6$  mice/group. C, quantification for the protein levels of ICAM-1 in heart samples of 8-month-old WT and TLR2-KO male mice. Data are presented as mean  $\pm$  S.D.; \*,  $p < 0.05$  with Student's  $t$  test used to calculate the  $p$  value. D, representative Western blot images showing the expression of TLR1, TLR2, TLR4, and TLR6 in the heart samples of 8-month-old WT and TLR2-KO male mice.  $n = 6$  mice/group. E, quantification of TLR1, TLR2, TLR4, and TLR6 protein levels in 8-month-old WT and TLR2-KO male mice heart samples assessed by Western blotting.  $n = 6$  mice/group. Data are presented as mean  $\pm$  S.D.; \*,  $p < 0.05$  with Student's  $t$  test used to calculate the  $p$  values. Note that TLR2 antibody on higher exposure gives a weak band in TLR2-KO mice heart. F, qPCR analysis of mRNA levels of TLR ligands in WT and TLR2-KO male mice heart samples.  $n = 6-8$  mice/group. Data are presented as mean  $\pm$  S.D.; \*,  $p < 0.05$  with Student's  $t$  test used to calculate the  $p$  values.

(47). Because we found reduced phosphorylation of FoxO in TLR2-KO mice, we suspected that TLR2-deficient cells might display increased nuclear levels of FoxO. As expected, we observed increased nuclear localization of FoxO1 in TLR2-deficient cardiomyocytes by confocal microscopy (Fig. 6, C and D). Similarly, we also noted increased nuclear localization of FoxO3a (data not shown). Next, we tested the transcriptional activity of FoxO in control and TLR2-KO cardiomyocytes. To

check the transcriptional activity of FoxO, we performed a luciferase assay in cardiomyocytes isolated from control and TLR2-KO mice using a plasmid construct carrying 6 $\times$  FoxO-binding sites. Consistent with our previous findings, we observed significantly higher transcriptional activity of FoxO in TLR2-deficient cardiomyocytes (Fig. 6E). However, cardiac fibroblasts isolated from TLR2-KO mice failed to show enhanced transcriptional activity of FoxO (Fig. S1A). These findings demonstrate that TLR2 deficiency impairs Akt signaling and thus activates the FoxO transcription factors. To further verify the increased transcriptional activation of FoxO, we performed a confocal analysis in TLR2-KO cardiomyocytes for the expression levels of ubiquitin, atrogin-1, MuRF-1, BAX, AIF, cleaved caspase-3, and ICAM-1, which are targets of FoxO transcription factors (48), and found that all these proteins showed increased expression in TLR2-KO cardiomyocytes (Fig. 6, F and G). However, the expression of FoxO target genes, *i.e.* BAX, caspase-3, and AIF, was not affected in TLR2-deficient cardiac fibroblasts (Fig. S1, B and C). These results indicate that TLR2 deficiency might have a significant impact on cardiomyocytes as compared with cardiac fibroblasts. Further, Western blot analysis for BAX and AIF, which are also FoxO target genes, show increased protein levels in TLR2-KO mice heart samples (Fig. 6, H and I). To further validate our findings, we tested the endogenous mRNA levels of the FoxO target cell cycle arrest and cell death genes p16, p21, p53, TRAIL, and GADD45A in control and TLR2-KO mice hearts. We observed significant up-regulation in the expression levels of p16, p21, p53, TRAIL, and GADD45A in TLR2-deficient hearts (Fig. 6J). Collectively, these findings indicate that TLR2 deficiency impairs Akt activity and thus enhances the transcriptional activity of FoxO to induce the expression of genes involved in cardiac atrophy and cell death.

### Inhibition of FoxO rescues the defects in TLR2-KO cardiomyocytes and TLR2-KO mouse hearts

Because TLR2-KO mice show a hyperactive FoxO transcription factor, we performed a series of rescue experiments to understand whether inhibition of FoxO attenuates the total protein ubiquitination and expression of atrogens in TLR2-deficient mice. In this experiment, we used neonatal cardiomyocytes isolated from TLR2-KO mice. It should be noted that neonatal cardiomyocytes may not mirror the aging phenotype found in mice. As our previous findings suggest that TLR2-KO neonatal cardiomyocytes show augmented FoxO activity, we inhibited the endogenous FoxO activity in cardiomyocytes by a dominant-negative FoxO-expressing adenovirus. When cardiomyocytes were infected with the dominant-negative FoxO adenovirus, we found an almost 50% reduction in transcriptional activity of endogenous FoxO, indicating that FoxO dominant-negative virus is functionally active (data not shown). We probed for the expression levels of MuRF-1, atrogin-1, and total cellular ubiquitin by confocal microscopy in control and TLR2-KO cardiomyocytes infected with dominant-negative FoxO adenovirus. We observed a significant down-regulation of total protein ubiquitination, atrogin-1, and MuRF-1 levels in TLR2-deficient cardiomyocytes following dominant-negative FoxO expression (Fig. 7, A and B). We per-



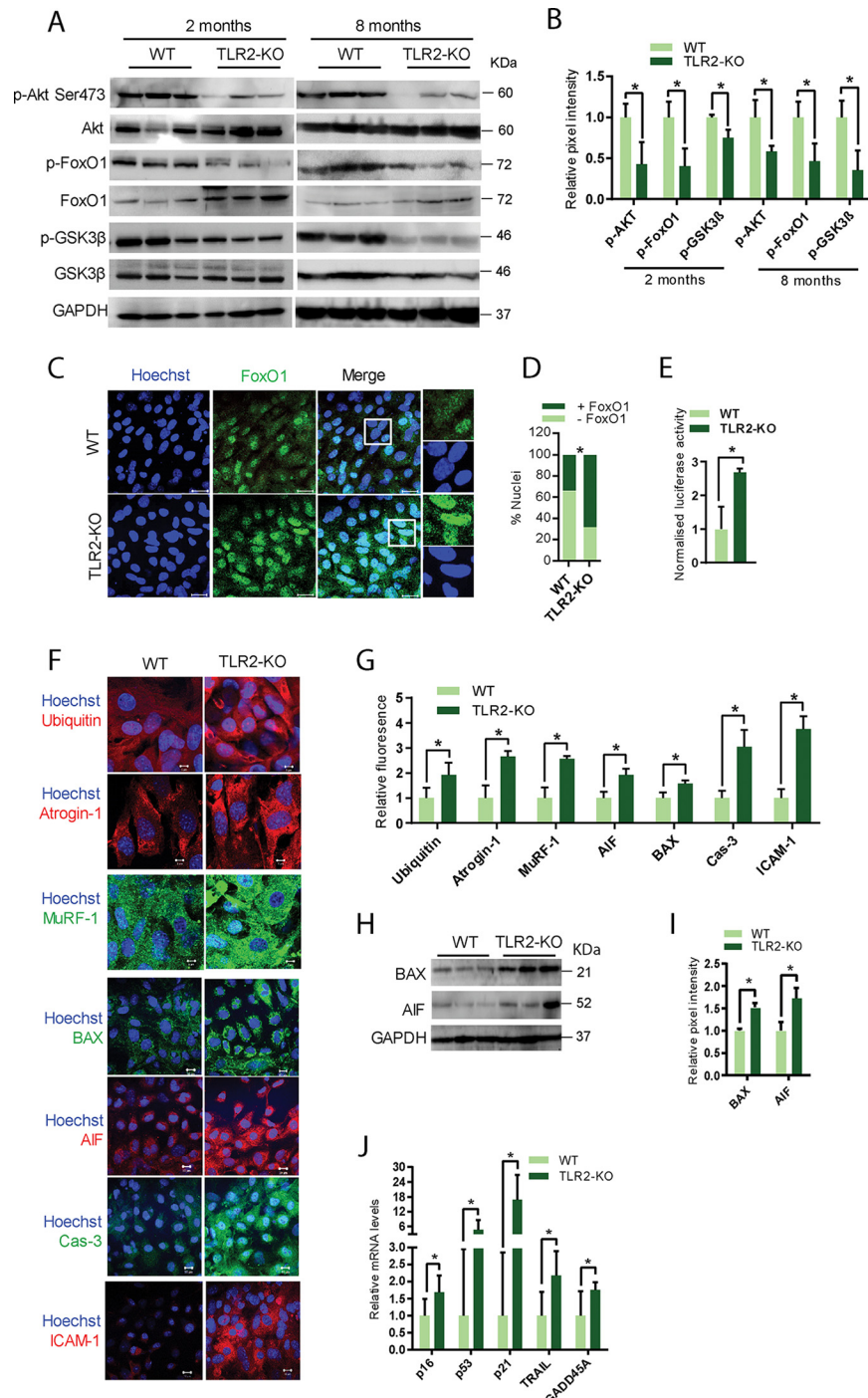


**Figure 6. TLR2 regulates FoxO via activation PI3K/Akt pathway.** *A*, representative Western blot images showing levels of indicated proteins in heart samples of 2-month- and 8-month-old WT and TLR2-KO male mice.  $n = 6$  mice/group. *B*, quantification of protein levels of p-Akt, p-FoxO1, and p-GSK3 $\beta$  in the heart samples of 2-month- and 8-month-old WT and TLR2-KO male mice.  $n = 6$  mice/group. Data are presented as mean  $\pm$  S.D.; \*,  $p < 0.05$  with Student's  $t$  test used to calculate the  $p$  values. *C*, representative confocal images showing WT and TLR2-KO cardiomyocytes stained with antibodies against FoxO1. Merged images (cyan) show nuclear (blue) presence of FoxO1 (green). Zoomed images show the increased nuclear levels of FoxO1 in TLR2-KO cardiomyocytes.  $n = 3$  independent experiments. Scale bar = 20  $\mu$ m. *D*, quantification of percentage of nuclei having FoxO1 in WT and TLR2-KO cardiomyocytes.  $n = 3$  independent experiments. \*,  $p < 0.05$  with Student's  $t$  test used to calculate the  $p$  values. *E*, graph showing luciferase reporter activity in WT and TLR2-KO cardiomyocytes transfected with FoxO-Luc plasmid. Renilla-Luc was used for normalization. Data are presented as mean  $\pm$  S.D.,  $n = 3$  independent experiments; \*,  $p < 0.05$  with Student's  $t$  test used to calculate the  $p$  values. *F*, representative confocal images of WT and TLR2-KO cardiomyocytes stained for FoxO downstream targets, i.e. ubiquitin, atrogin-1, MuRF-1, BAX, AIF, cleaved caspase-3 (Cas-3) and ICAM-1.  $n = 3$  independent experiments. *G*, quantification of the expression levels as seen with confocal microscopy of the FoxO downstream targets, i.e. ubiquitin, atrogin-1, MuRF-1, BAX, AIF, Cas-3 and ICAM-1.  $n = 3$  independent experiments. Data are presented as mean  $\pm$  S.D.; \*,  $p < 0.05$  with Student's  $t$  test used to calculate the  $p$  values. *H*, representative Western blot images showing the expression of BAX and AIF in heart samples of 8-month-old WT and TLR2-KO male mice.  $n = 6$  mice/group. Data are presented as mean  $\pm$  S.D.; \*,  $p < 0.05$  with Student's  $t$  test used to calculate the  $p$  values. *I*, quantification for the protein levels of BAX and AIF in heart samples of 8-month-old WT and TLR2-KO male mice.  $n = 6$  mice/group. Data are presented as mean  $\pm$  S.D.; \*,  $p < 0.05$  with Student's  $t$  test used to calculate the  $p$  values. *J*, qPCR analysis of the mRNA levels of FoxO downstream targets, i.e. p21, p16, p53, TRAIL, and GADD45a in 8-month-old WT and TLR2-KO male mice heart samples. RPL32 was used as the housekeeping gene.  $n = 7-12$  mice/group. Data are presented as mean  $\pm$  S.D.; \*,  $p < 0.05$  with Student's  $t$  test used to calculate the  $p$  values.

## TLR2 deficiency induces aging-related heart failure

formed *in vivo* rescue experiments by injecting control and TLR2 knockout mice with the FoxO1 inhibitor AS1842856 to further validate our findings. Our results suggest that inhibition of FoxO1 significantly reduced the HW/BW and HW/TL ratios, as well as the LVID, and improved the wall thickness and fractional shortening in TLR2-KO mice (Fig. 7, C–G). These observations indicate that hyperactivation of FoxO1 is responsible for the adverse remodeling and contractile dysfunction in TLR2-KO mice. To test whether the observed phenotype is associated with changes in the expression of FoxO target muscle wasting and cell death genes, we performed Western blot analysis for the levels of MuRF-1, atrogin-1, and TRAIL in vehicle and inhibitor-treated TLR2-KO mice. We found that the protein amounts of MuRF-1, atrogin-1, and TRAIL were reduced significantly in TLR2-KO mice following FoxO1 inhibitor treatment (Fig. 7, H and I). Collectively, our data indicate that the hyperactivation of FoxO transcription factors is responsible for the development of aging-related adverse remodeling and contractile dysfunction in TLR2-KO mice.

### Activation of TLR1/2 signaling improved contractile functions of aged mice

As TLR2-KO mice develop aging-related heart failure, we tested whether TLR2 plays any role in aging-related decline in the cardiac function of aged mice. First, we assessed the expression of TLR2 and phosphorylation of Akt in young and old mice. Interestingly, the protein levels of TLR2 was significantly lower in the heart tissues of aged mice, which was correlated with reduced phosphorylation of Akt (Fig. 8, A and B). Next, we tested whether activation of TLR2 signaling by Pam<sub>3</sub>CSK<sub>4</sub>, an agonist of TLR1/2 signaling (49), would improve heart functions. Short-term treatment with Pam<sub>3</sub>CSK<sub>4</sub> markedly improved the macrophages levels in the heart tissues of aged mice (Fig. 8, C and D). However, Pam<sub>3</sub>CSK<sub>4</sub> treatment failed to up-regulate the serum cytokine levels (Fig. 8E), suggesting that Pam<sub>3</sub>CSK<sub>4</sub> at this dose did not elicit any systemic immune response. Assessment of cardiac structure and function indicated that Pam<sub>3</sub>CSK<sub>4</sub> treatment did not alter either the ventricular wall thickness or LVID. However, Pam<sub>3</sub>CSK<sub>4</sub> treatment significantly improved the contractile functions of the heart as assessed by echocardiography (Fig. 8, F–H). These findings suggest that activation of TLR signaling might improve the contractile functions of the heart in aged mice.

### Discussion

In the present study, we found that TLR2-deficient mice developed accelerated aging-associated cardiac remodeling and dysfunction, which closely resembles heart failure during aging. We found that TLR2-deficient hearts show impaired Akt activity, thus increasing the transcriptional activity of FoxO transcription factors. FoxO hyperactivation lead to transcriptional up-regulation of genes involved in cell death and cardiac muscle wasting, which might have induced heart failure in TLR2-KO mice. We also found that TLR2 levels decreased during aging, and activation of TLR1/2 signaling improved cardiac function in aged mice.

In our work, we have demonstrated the development of age-dependent cardiac remodeling and dysfunction in TLR2-KO mice. Our data indicate that TLR2-deficient mice are obese even at 2 months of age, as reported previously (22). TLR2 deficiency increases the susceptibility to high-fat diet-induced obesity (22). A previous work identifies ventricle enlargement, a hallmark of schizophrenia, in the brains of TLR2-KO mice (50). Along similar lines, TLR2-deficient mice develop severe colitis in an aging-dependent manner (23), indicating that TLR2-deficient mice are susceptible to aging-related diseases. These findings are in contrast to earlier reports in which TLR2-deficient mice were protected from *S. aureus*- or doxorubicin-induced cardiac dysfunction, myocardial infarction, and atherosclerosis (20). However, it is worth mentioning that these studies were conducted with young TLR2-KO mice. In our study, we found cardiac dysfunction in TLR2-KO mice, accompanied by increased cell death. Like our findings, a previous work has shown that blocking TLR2 signaling increases cell death following oxidative stress in rat cardiomyocytes (15). Therefore, loss of TLR2 seems to be detrimental and would increase the susceptibility of cardiomyocytes to aging and stress.

TLR2 activation has been shown to activate the TLR2/PI3K/Akt pathway in the brain (51). In chronic heart failure patients, IGF-1/Akt signaling has been reported to be down-regulated, leading to muscle wasting of the heart (52). Previous reports have shown up-regulated transcriptional activity of FoxO1 in failing hearts in humans and mice (31). This is in accordance with our study, where we found increased FoxO levels in a TLR2-deficient background, which in turn lead to the development of heart failure. Classical studies conducted using transgenic animal models indicate that the targeting of Akt to the nucleus inhibits apoptosis and preserves cardiac functions during heart failure (52). Similarly, inhibition of Akt by overexpression of a dominant-negative PI3K mutant or ablation of Akt in the heart results in a lack of adaptive responses to the stress. Thus, the cardioprotective effects displayed by the TLR agonists are attributed to the induction of PI3K/Akt signaling (53).

Generally, TLR2 forms heterodimers with either TLR1 or TLR6 on the cell surface to recognize a variety of endogenous and exogenous ligands (54, 55). The phenomenon of TLR2 heterodimerization expands the ligand spectrum but does not essentially induce differential signaling (56). Interestingly, TLR2/6 but not TLR1/2 heterodimers bind to Junin virus glycoprotein to initiate the immune response (57). On similar lines, the Meningococcal porin PorB interacts with TLR2 and initiates signaling via TLR1 (58). The heterodimers of TLR2/6 or TLR1/2 are necessary for ligand-dependent signal activation, and homodimers of TLR2 or TLR1 are incapable of initializing signaling (54). Still, it is unclear whether TLR1 or TLR6 can activate host immune response in the absence of TLR2 involvement (59). In our work, we found that TLR1 levels were high in TLR2-KO mice. However, the compensatory up-regulation of TLR1 in the TLR2-KO mice may not result in any functional phenotype, as TLR1 homodimers are incapable of activating the TLR signaling.

TLR ligands, including heat shock proteins and HMGB1, are released from senescent cells via exosomes (60, 61). These TLR

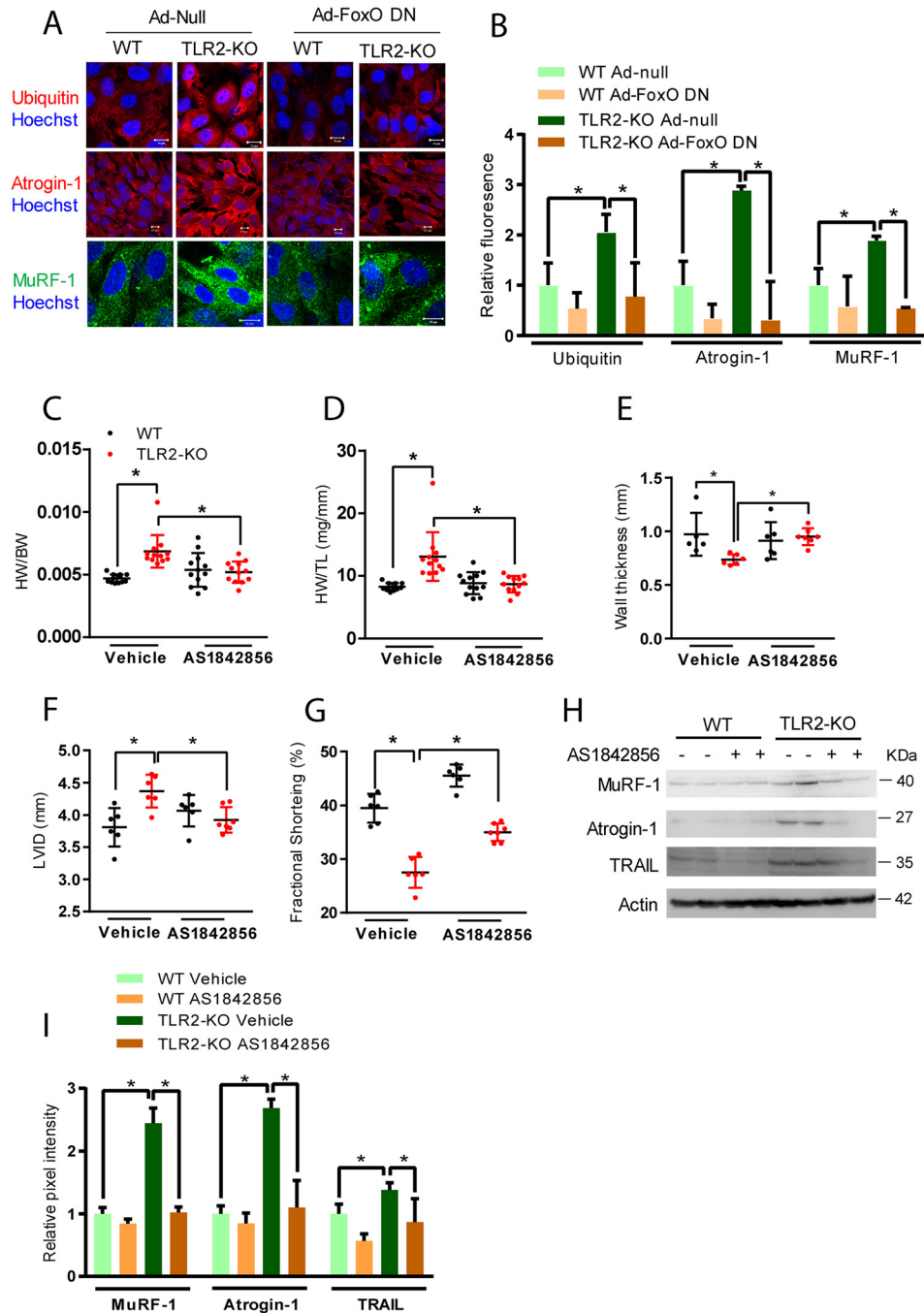


**Figure 7. Inhibition of FoxO1 rescues the phenotype of TLR2-depleted cardiomyocytes and TLR2-KO mice.** *A*, representative confocal images of WT and TLR2-KO cardiomyocytes infected with control adenovirus (*Ad-Null*) or dominant-negative FoxO adenovirus (*Ad-FoxO DN*) stained with antibodies against ubiquitin, atrogin-1, and MuRF-1. *n* = 3 independent experiments. Scale bar = 10  $\mu$ m. *B*, quantification for the levels of expression of ubiquitin, MuRF-1, and atrogin-1 in WT and TLR2-KO primary cardiomyocytes infected with either control adenovirus or dominant-negative FoxO adenovirus. *n* = 3 independent experiments. Data are presented as mean  $\pm$  S.D.; \*, *p* < 0.05 with one-way ANOVA used to calculate the *p* values. *C*, graph showing HW/BW ratio of 12-month-old WT and TLR2-KO male mice injected with either vehicle or FoxO1 inhibitor AS1842856. *n* = 12 mice/group. Data are presented as mean  $\pm$  S.D.; \*, *p* < 0.05 with one-way ANOVA used to calculate the *p* values. *D*, graph depicting HW/TL (mg/mm) of 12-month-old WT and TLR2-KO male mice injected with either vehicle or FoxO1 inhibitor AS1842856. *n* = 12 mice/group. Data are presented as mean  $\pm$  S.D.; \*, *p* < 0.05 with one-way ANOVA used to calculate the *p* values. *E*, graph representing left ventricular posterior wall thickness (mm) at diastole of 12-month-old WT and TLR2-KO male mice injected with either vehicle or FoxO1 inhibitor AS1842856. *n* = 6 mice/group. Data are presented as mean  $\pm$  S.D.; \*, *p* < 0.05 with one-way ANOVA used to calculate the *p* values. *F*, graph showing left ventricular internal diameter (mm) during diastole of 12-month-old WT and TLR2-KO male mice injected with either vehicle or FoxO1 inhibitor AS1842856. *n* = 6 mice/group. Data are presented as mean  $\pm$  S.D.; \*, *p* < 0.05 with one-way ANOVA used to calculate the *p* values. *G*, graph showing the contractile functions of heart as represented by fractional shortening (%) of 12-month-old WT and TLR2-KO male mice injected with either vehicle or FoxO1 inhibitor AS1842856. *n* = 6 mice/group. Data are presented as mean  $\pm$  S.D.; \*, *p* < 0.05 with one-way ANOVA used to calculate the *p* values. *H*, Western blot analysis for FoxO target genes MuRF-1, atrogin-1, and TRAIL in heart samples of 12-month-old WT and TLR2-KO male mice treated with either vehicle or FoxO1 inhibitor AS1842856. *n* = 6 mice/group. *I*, quantification for the protein levels of FoxO target genes MuRF-1, atrogin-1, and TRAIL in heart samples of 12-month-old WT and TLR2-KO male mice treated with either vehicle or FoxO1 inhibitor AS1842856. *n* = 6 mice/group. \*, *p* < 0.05 with one-way ANOVA used to calculate the *p* values.



## TLR2 deficiency induces aging-related heart failure

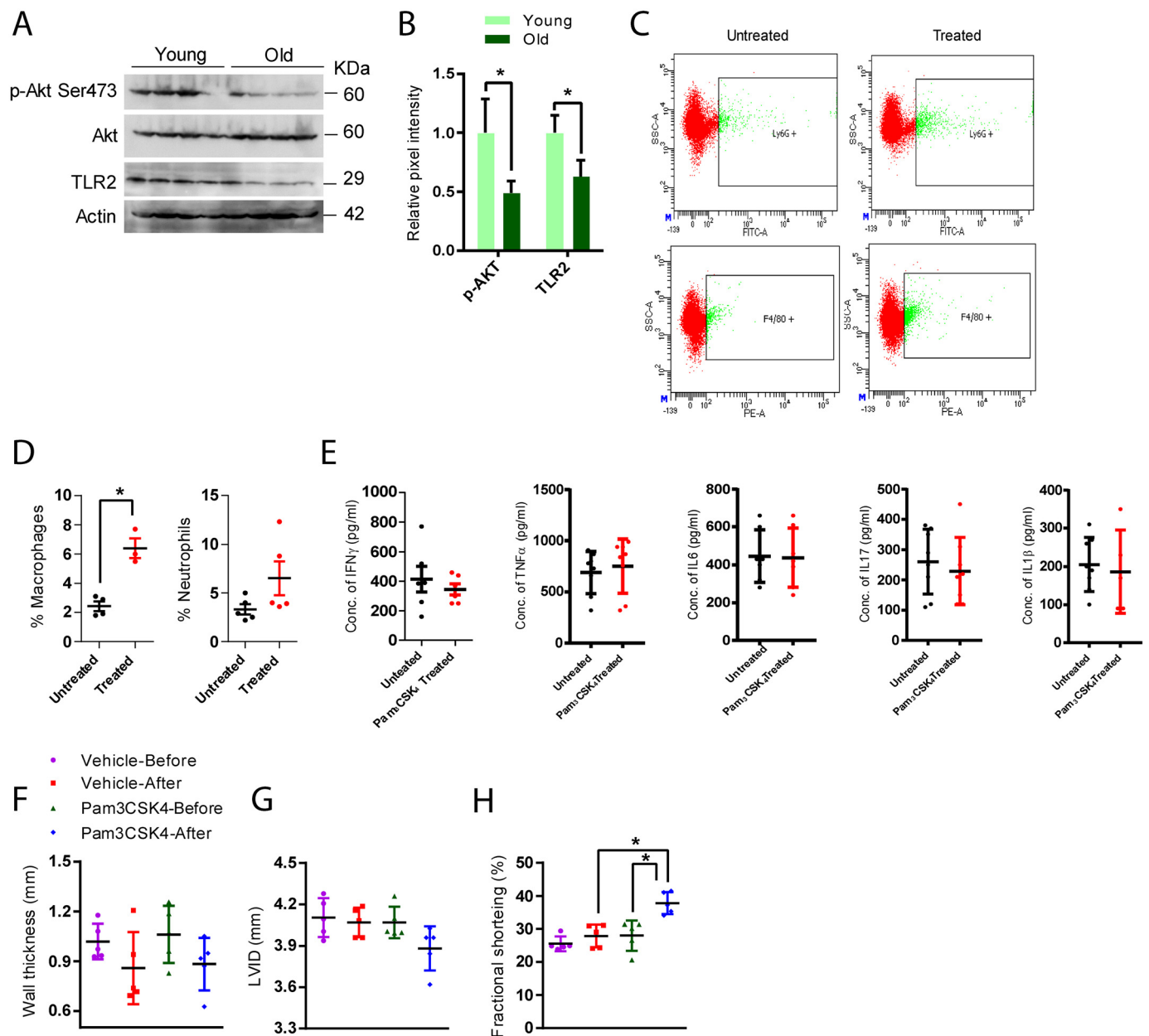


**Figure 8. TLR2 expression reduces with aging in mice and activation of TLR improves contractile functions of mice.** *A*, representative Western blot images showing the expression of the indicated proteins in heart samples of mice at 2 months (Young) and 12 months (Old) of age. *n* = 4 mice/group. *B*, quantification of the phospho-Akt and TLR2 levels in heart samples of mice at 2 months (Young) and 12 months (Old) of age. *n* = 4 mice/group. \*, *p* < 0.05 with Student's *t* test used to calculate the *p* values. *C*, representative scatter plots showing the Ly6G-positive neutrophils (green, FITC staining) and F4/80-positive macrophages (red, PE staining) in heart tissues of 12-month-old WT mice treated with either vehicle or Pam<sub>3</sub>CSK<sub>4</sub>. Pam<sub>3</sub>CSK<sub>4</sub> was injected i.p. in mice at 100  $\mu$ g/dose/mice every 48 h for 10 days. *D*, graph showing percentage of neutrophils and macrophages assessed by flow cytometry in heart tissues of 12-month-old WT mice treated with either vehicle (Untreated) or Pam<sub>3</sub>CSK<sub>4</sub> (Treated). *n* = 5 mice/group. Data are presented as mean  $\pm$  S.D.; \*, *p* < 0.05 with Student's *t* test used to calculate the *p* value. *E*, analysis of serum cytokine profile in 12-month-old WT mice treated with either vehicle or Pam<sub>3</sub>CSK<sub>4</sub> assessed by ELISA. *n* = 5–8 mice/group. Data are presented as mean  $\pm$  S.D.; \*, *p* < 0.05 with Student's *t* test used to calculate the *p* value. *F*, graph representing left ventricular posterior wall thickness (mm) at diastole of 12-month-old WT mice before and after treatment with either vehicle or Pam<sub>3</sub>CSK<sub>4</sub>. *n* = 5 mice/group. Data are presented as mean  $\pm$  S.D.; \*, *p* < 0.05 with one-way ANOVA used to calculate the *p* values. *G*, graph showing LVID (mm) during diastole of 12-month-old WT mice before and after treatment with either vehicle or Pam<sub>3</sub>CSK<sub>4</sub>. *n* = 5 mice/group. Data are presented as mean  $\pm$  S.D.; \*, *p* < 0.05 with one-way ANOVA used to calculate the *p* values. *H*, graph showing the contractile functions of heart as represented by fractional shortening (%) of 12-month-old WT before and after treatment with either vehicle or Pam<sub>3</sub>CSK<sub>4</sub>. *n* = 5 mice/group. Data are presented as mean  $\pm$  S.D.; \*, *p* < 0.05 with one-way ANOVA used to calculate the *p* values.

ligands can be also released from cells that are undergoing necrosis. After release, the heat shock proteins and HMGB1 binds to innate immune receptors, especially TLR2 and TLR4 situated on resident immune cells. Interestingly, they can also bind directly to several other surface receptors such as CD91, scavenger receptors, CD40, and CCR5 to promote inflamma-

tory responses in neighboring tissues (62, 63). Our findings suggest that the expression of TLR agonists is high in the heart tissue of TLR2-KO mice. The increased level of heat shock proteins and HMGB1 may be an attempt to enhance inflammatory responses in the heart of TLR2-KO mice. This hypothesis is consistent with our observation that TLR2-KO mice hearts

express enhanced expression of cell adhesion molecules ICAM-1, VCAM-1, and MCP-1 and show augmented cell death.

Macrophages, apart from their well-documented role in tissue homeostasis and host defense, play a critical role in pathophysiological processes induced by myocardial infarction (64). Macrophages facilitate the conduction of electrical impulses in the heart (65). A reduction in the number of macrophages in the heart after infarction in mice has been reported to correlate with increased mortality and impaired cardiac repair (66). Interestingly, TLR2 deficiency is associated with reduced immune cells infiltration in the heart (67). Mice treated with anti-TLR2 antibody have reduced macrophage infiltration. Similar results were obtained in our study, where we observed reduced infiltration of macrophages in the hearts of TLR2-KO mice, even though up-regulation of MCP-1 was observed. The improvement of cardiac function in aged mice by TLR1/2 agonist treatment is associated with an increased number of macrophages and neutrophils in the heart.

TLR signaling has been reported to be impaired with aging (24). Decreased surface expression of TLR1 has been reported to be strongly associated with the reduction in the production of cytokines (68). Further, aging-associated immune response impairment can be seen with the decline in delayed-type hypersensitivity response (69). In other cases, an alteration in TLR response due to aging has been reported to contribute to an increase in the risk of infectious diseases (70). One of the probable mechanisms of impaired TLR signaling in the context of human aging is a decrease in PI3K activity, which is associated with an increase in the phosphorylation of PTEN (71) and impaired down-regulation of phosphorylation of STAT1 in macrophages (70). These events are responsible for an increase in TLR-dependent cytokine production during aging (24). In contrast, aging-associated decline in TLR expression and signaling have been reported in murine models, which in turn is associated with impaired phosphorylation of MAP kinase (68). We found that TLR2 levels are reduced in aged mice hearts. Based on current findings, we argue that the age-related defect in TLR signaling in macrophages may play a major role in the development of age-dependent cardiac dysfunction in TLR2-KO mice.

Major studies regarding polymorphisms in TLRs have been carried out on a specific TLR4 polymorphism D299G (24). Some studies show that this SNP is associated with impaired lipopolysaccharide-induced signaling (72, 73). In contrast, other studies carried out in primary human cells isolated from heterozygous individuals for D299G SNP show either unchanged or increased lipopolysaccharide-induced cytokine response (73–76). Moreover, attenuated inflammation in cases of diminished TLR4 function result in decreased TLR responsiveness (77). The authors of this study report that in a set of Sicilian subjects, the SNP D299G was over-represented in people at the age of 100 or older but under-represented in patients with acute myocardial infarction (77). However, future studies will be required to understand the role of TLR2 signaling in the development of heart failure and other aging-related diseases in humans.

Overall, our findings indicate that the loss of TLR2 is detrimental to the heart. We believe that the observed cardiomyopathy phenotype might be a combined effect of a TLR2 defect in cardiomyocytes and immune cells, as we found more cell death, atrophy, and fibrosis in TLR2-KO hearts. Because TLR2 is expressed in most of the cell types of the heart, future studies will be required to address the cell-specific role of TLR2 in the maintenance of cardiac homeostasis.

## Experimental procedures

### Animals, cell culture, reagents, and methods

All animal protocols were carried out with the approval of institutional animal ethics committee of the Indian Institute of Science, Bengaluru, constituted as per Article 13 of the Committee for Control and Supervision of Experiments on Animals (CPCSEA), Government of India. All of the studies conformed with the Update for the Care and Use of Laboratory Animals, Guide for the Care and Use of Laboratory Animals, 8th edition, published by the U. S. National Institutes of Health (NIH Publication 2011). TLR2-KO mice were purchased from The Jackson Laboratory (B6.129-Tlr2<sup>tm1Kir</sup>/J, stock No. 004650). These TLR2-KO mice are deficient in TLR2 in all cell types. Animals were housed in the clean-air facility of the Indian Institute of Science in individually ventilated cages with food and water *ad libitum*. Genotyping was used to confirm the genetic modification for each mouse used in the study. A CO<sub>2</sub> chamber was used for sacrificing the mice, and heart tissues were harvested. Primary cardiomyocytes were isolated from the neonatal WT and TLR2-KO mice as per the previously described protocol (78). Adenovirus for dominant-negative FoxO expression was a kind gift from Mahesh P. Gupta, University of Chicago. Mice were injected daily for 10 days with FoxO1 inhibitor AS1842856 (Millipore) at a dose of 5 mg/kg for *in vivo* rescue experiments. Pam<sub>3</sub>CSK<sub>4</sub>, a TLR1/2 agonist, was injected i.p. in mice at 100 µg/dose/mice every 48 h for 10 days.

### Western blot analysis

A previously reported protocol was used for Western blotting (79). Mice heart tissue and cell lysates were prepared with lysis buffer containing 1 mM EDTA, 1 mM EGTA, 50 mM Tris-HCl, pH 7.8, 1% Nonidet P-40, 150 mM NaCl, 0.5% sodium deoxycholate, and 1% SDS supplemented with sodium orthovanadate, sodium pyrophosphate, a protease inhibitor mixture (Sigma), and phenylmethylsulfonyl fluoride. Bradford assay was used to determine the protein concentration. The antibodies used are as follows: fibronectin-1 (Santa Cruz Biotechnology),  $\alpha$ -smooth muscle actin (Sigma-Aldrich), periostin (Cloud-Clone Corp.), ANP (Cloud-Clone Corp.), cleaved caspase-3 (Santa Cruz Biotechnology), PARP-1 (Santa Cruz Biotechnology), BAX (Santa Cruz Biotechnology), AIF (Thermo Scientific), ubiquitin (Millipore), ICAM-1 (DSHB), Atrogin-1 (Thermo Scientific), Akt1/2/3 (Santa Cruz Biotechnology), p-Akt (Ser-473) (Cell Signaling Technology), GSK-3 $\beta$  (Cell Signaling Technology), and p-GSK-3 $\beta$  (Cell Signaling Technology). GAPDH (Santa Cruz Biotechnology) and HRP-actin (Cell Signaling Technology) were used as the loading control. The blots were developed using ECL reagents in a ChemiDoc Touch chemiluminescence detection system (Bio-Rad).

## TLR2 deficiency induces aging-related heart failure

### Confocal microscopy

Our previous publications describe the detailed protocol for immunofluorescence (79). Paraformaldehyde (3.7%) was used for fixing cells, and 0.2% Triton X-100 was used for permeabilization. Following incubation with the respective primary antibodies, cells were incubated with secondary antibodies conjugated with Alexa Fluor 488 and/or 546 (Thermo Scientific). The primary antibodies used were FoxO-1 (Cell Signaling Technologies), ubiquitin (Millipore), atrogin-1 (Cloud-Clone Corp.), MuRF-1 (Santa Cruz Biotechnology), BAX (Santa Cruz Biotechnology), AIF (Thermo Scientific), caspase-3 (Santa Cruz Biotechnology), and ICAM-1 (Cloud-Clone Corp.). The nuclei were stained using Hoechst. A Carl Zeiss LSM 710 confocal microscope was used to acquire images.

### Luciferase reporter assay

The cells were transfected with FoxO-Luciferase reporter plasmid with 6× FoxO-binding sites using Lipofectamine 2000 (Invitrogen). A Renilla-Luc reporter plasmid was used for normalization. A luminometer was used to measure the luminescence (Pharmingen Moonlight 3010, BD Biosciences).

### Histology and immunohistochemistry

Age-matched WT and TLR2-KO mice hearts were collected and were immediately fixed in 10% neutral buffered formalin. Tissue processing was done with an automated tissue processor (Leica Biosystems, Wetzlar, Germany). Paraffin-embedded 4- $\mu$ m-thick tissue sections were stained with Masson's trichrome stain (Sigma) to observe and measure fibrosis. Fibrosis was scored in the sections on a scale of 1 to 5, with 5 indicating maximum fibrosis. Hematoxylin and eosin staining was done to score macrophage infiltration and atrophy in control and TLR2-KO mice hearts. Myocyte cell size was measured using sections stained with WGA (Invitrogen, 5  $\mu$ g/ml). For immunohistochemistry, formalin-fixed paraffin-embedded tissue sections (5- $\mu$ m thick) were cut and mounted on poly-L-lysine (Sigma-Aldrich)-coated slides and air-dried for 30 min. Anti-periostin and anti-CD-163 hyperimmune serum raised in rabbit (Cloud-Clone Corp.) were diluted to 1:150 in 1% BSA, and goat anti-rabbit IgG-HRP conjugate (Santa Cruz Biotechnology) was used as the secondary antibody at a 1:150 dilution in PBS. 3,3'-Diaminobenzidine (DAB, Abcam) substrate was prepared as per the manufacturer's recommendation, and counterstaining was done with methyl green. DAB-stained sections were mounted with DPX mountant (Sigma-Aldrich). For the negative control, the primary antibody was substituted by 1% BSA, and other procedures were followed as mentioned above. A TUNEL assay was performed according to the manufacturer's protocol (Abcam).

### Echocardiography of mice

Mice were anesthetized through isoflurane (~1%) inhalation. The chest hair of the mice was removed using a topical depilatory agent. For electrogram grating, limb leads were attached, and a VisualSonics Vevo 1100 machine was used to image the animals in the left lateral decubitus position. A heated imaging platform along with warming lamps was used to

maintain the body temperature of the animals. Left ventricular chamber size and the wall thickness were measured, and fractional shortening was calculated.

### Real-time qPCR analysis

Protocol for real-time qPCR has been described in our previous publication (79). The primer sequences used were as follows: ANP forward, 5'-CCTGTGTACAGTGCGGTGTC-3', and reverse, 5'-CCTCATCTTCTACCGGCATC-3'; BNP forward, 5'-AAGGGAGAATACGGGCATCATTG-3', and reverse, 5'-ACAGCACCTTCAGGAGATCCA-3';  $\alpha$ -MHC forward, 5'-TAAAAATTGAGGACGAGCAGGC-3', and reverse, 5'-TCCAGCTCCTCGATGCGTGCC-3';  $\beta$ -MHC forward, 5'-AGCAGCAGTTGGATGAGCGACT-3', and reverse, 5'-CCAGCTCCTCGATGCGTGCC-3'; TRAIL forward, 5'-CGGAGAAGCACTCAGCTTTA-3', and reverse, 5'-GTTGAGAAATGAATGCCCTTTCC-3'; GADD45A forward, 5'-GACATCAACATCTGCGGGT-3', and reverse, 5'-TGAATGTGGGTTCGTCACCAG-3'; ICAM-1 forward, 5'-TACGTGTGCCATGCCTTTAGC-3', and reverse, 5'-GCCCCACATTGACCAGCAGTA-3'; VCAM-1 forward, 5'-TCTCTCAGGAAAGTCCACCC-3', and reverse, 5'-CACAGCCAATAGCAGCACAC-3'; MCP-1 forward, 5'-CCACAACCACCTCAAGCACT-3', and reverse, 5'-TAAGGCATCACAGTCCGAGTC-3'; atrogin-1 forward, 5'-AGCGCTTCTTGATGAGAAA-3', and reverse, 5'-GGCAGTCGAGAAGTCCAGTC-3'; MuRF-1 forward, 5'-TGCC-TGGAGATGTTTACCAAGC-3', and reverse, 5'-AAACGACCTCCAGACATGGACA-3'; p16 forward, 5'-CGTACCCCGATTTCAGGTGATG-3', and reverse, 5'-AGAAGGTAGTGGGTCCCTCG-3'; p21 forward, 5'-GACAAGAGGCCCACTTCT-3', and reverse, 5'-GCTTGGAGTGATAGAAATATGTC-3'; p53 forward, 5'-CACAGCGTGGTGGTACCTTA-3', and reverse, 5'-TCTTCTGTACGGCGGTCTCT-3'; and GAPDH forward, 5'-TATGTCGTGGAGTCTACTGGT-3', and reverse, 5'-GAGTTGTCATATTTCTCGTGG-3'.

### Flow cytometry analysis

Whole hearts from WT and TLR2 knockout mice were digested as described earlier (80). A previously described protocol was followed for the staining of isolated cells (81). A single-cell suspension of cells isolated from the heart was washed and resuspended in a blocking buffer composed of 2.5% BSA, 5% fetal calf serum, and a 1:200 dilution of purified rat anti-mouse CD16/CD32 antibody (catalogue No. 553141, BD Pharmingen<sup>TM</sup>). Anti-mouse F4/80-PE (catalogue No. 12-4801-82, eBioscience) and anti-mouse Ly-6G-FITC (catalogue No. 551460, BD Pharmingen<sup>TM</sup>) were added to the cell suspensions to stain for macrophages and neutrophils, respectively. The cells were kept at 4°C for 45 mins in the dark and washed subsequently with PBS. The cells were then resuspended in PBS and acquired on a BD FACSVerse<sup>TM</sup> flow cytometer. Unstained and single fluorochrome-stained cells were used to set the baseline instrument application and compensation settings. Approximately 50,000 events were acquired on the singlet (forward scatter area *versus* forward scatter height) and live gate (forward scatter area *versus* side scatter area (SSC-A)). Using the unstained samples as reference, the gates for PE-positive (macrophages) and FITC-positive (neutrophils) cells



were set, and the respective cell populations were quantified. The results were analyzed using the software BD FACSDiva™ (BD Biosciences) and are depicted as SSC-A versus FITC/PE contour plots.

### Serum cytokine analysis

Blood was collected by cardiac puncture from age-matched WT and TLR2-KO mice. Blood was allowed to clot at room temperature for 2 h, and serum was separated by centrifugation at 3000 rpm for 10 min. The amounts of proinflammatory cytokines, e.g. IFN $\gamma$ , TNF $\alpha$ , IL6, IL17, and IL1 $\beta$  (1:10 dilution), were estimated in sera using sandwich ELISA kits from eBioscience. The final optical density reading was obtained at 450 nm using an ELISA plate reader (Molecular Devices) with appropriate standards (31.25–2000 pg/ml) for each cytokine and chemokine.

### Quantification and statistical analysis

Data analysis and graph preparation were performed using GraphPad Prism. Confocal images were analyzed using the image analysis software ZEN. Densitometric analysis of Western blotting and confocal images were performed using ImageJ software.

**Author contributions**—K. M. S., M. S., S. Mishra, P. A. D., S. Y., S. R., S. Maity, A. K. T., S. K., S. Majumdar, A. J., A. R., and D. K. data curation; K. M. S., M. S., S. Mishra, P. A. D., S. Y., S. R., S. Maity, A. K. T., S. K., S. Majumdar, A. J., A. R., and D. K. formal analysis; K. M. S., S. Maity, and N. R. S. funding acquisition; K. M. S., M. S., S. Mishra, P. A. D., S. Majumdar, and N. R. S. investigation; K. M. S., M. S., P. A. D., S. R., S. Maity, S. K., A. J., D. N., and N. R. S. methodology; S. Mishra and S. K. writing—original draft; S. Mishra and N. R. S. writing—review and editing; A. K. T., I. S., R. J. S., S. G. R., D. N., and N. R. S. resources; N. R. S. conceptualization; N. R. S. supervision.

### References

- Mann, D. L. (2011) The emerging role of innate immunity in the heart and vascular system: For whom the cell tolls. *Circ. Res.* **108**, 1133–1145 [CrossRef Medline](#)
- Fernández-Ruiz, I. (2016) Immune system and cardiovascular disease. *Nat. Rev. Cardiol.* **13**, 503 [CrossRef Medline](#)
- Bozkurt, B., Kribbs, S. B., Clubb, F. J., Jr, Michael, L. H., Didenko, V. V., Hornsby, P. J., Seta, Y., Oral, H., Spinale, F. G., and Mann, D. L. (1998) Pathophysiologically relevant concentrations of tumor necrosis factor- $\alpha$  promote progressive left ventricular dysfunction and remodeling in rats. *Circulation* **97**, 1382–1391 [CrossRef Medline](#)
- Anker, S. D., and von Haehling, S. (2004) Inflammatory mediators in chronic heart failure: An overview. *Heart* **90**, 464–470 [CrossRef Medline](#)
- Gage, J. R., Fonarow, G., Hamilton, M., Widawski, M., Martínez-Maza, O., and Vredevoe, D. L. (2004) Beta blocker and angiotensin-converting enzyme inhibitor therapy is associated with decreased Th1/Th2 cytokine ratios and inflammatory cytokine production in patients with chronic heart failure. *Neuroimmunomodulation* **11**, 173–180 [CrossRef Medline](#)
- Chung, E. S., Packer, M., Lo, K. H., Fasanmade, A. A., Willerson, J. T., and Anti-TNF Therapy Against Congestive Heart Failure Investigators (2003) Randomized, double-blind, placebo-controlled, pilot trial of infliximab, a chimeric monoclonal antibody to tumor necrosis factor- $\alpha$ , in patients with moderate-to-severe heart failure: results of the Anti-TNF Therapy Against Congestive Heart Failure (ATTACH) trial. *Circulation* **107**, 3133–3140 [CrossRef Medline](#)
- Takeda, K., and Akira, S. (2005) Toll-like receptors in innate immunity. *Int. Immunol.* **17**, 1–14 [Medline](#)
- Medzhitov, R. (2001) Toll-like receptors and innate immunity. *Nat. Rev. Immunol.* **1**, 135–145 [CrossRef Medline](#)
- Frantz, S., Ertl, G., and Bauersachs, J. (2007) Mechanisms of disease: Toll-like receptors in cardiovascular disease. *Nat. Clin. Pract. Cardiovasc. Med.* **4**, 444–454 [CrossRef Medline](#)
- Tang, A. H., Brunn, G. J., Cascalho, M., and Platt, J. L. (2007) Pivotal Advance: Endogenous pathway to SIRS, sepsis, and related conditions. *J. Leukocyte Biol.* **82**, 282–285 [CrossRef Medline](#)
- Yu, L., Wang, L., and Chen, S. (2010) Endogenous toll-like receptor ligands and their biological significance. *J. Cell Mol. Med.* **14**, 2592–2603 [CrossRef Medline](#)
- Higashikuni, Y., Tanaka, K., Kato, M., Nureki, O., Hirata, Y., Nagai, R., Komuro, I., and Sata, M. (2013) Toll-like receptor-2 mediates adaptive cardiac hypertrophy in response to pressure overload through interleukin-1 $\beta$  upregulation via nuclear factor  $\kappa$ B activation. *J. Am. Heart Assoc.* **2**, e000267 [CrossRef Medline](#)
- Wang, L., Li, Y. L., Zhang, C. C., Cui, W., Wang, X., Xia, Y., Du, J., and Li, H. H. (2014) Inhibition of Toll-like receptor 2 reduces cardiac fibrosis by attenuating macrophage-mediated inflammation. *Cardiovasc. Res.* **101**, 383–392 [CrossRef Medline](#)
- Pop-Moldovan, A. L., Trofenciu, N. M., Drbanu, D. A., Precup, C., Branea, H., Christodorescu, R., and Puchi, M. (2017) Customized laboratory TLR4 and TLR2 detection method from peripheral human blood for early detection of doxorubicin-induced cardiotoxicity. *Cancer. Gene. Ther.* **24**, 203–207 [CrossRef Medline](#)
- Frantz, S., Kelly, R. A., and Bourcier, T. (2001) Role of TLR-2 in the activation of nuclear factor  $\kappa$ B by oxidative stress in cardiac myocytes. *J. Biol. Chem.* **276**, 5197–5203 [CrossRef Medline](#)
- Chao, W. (2009) Toll-like receptor signaling: A critical modulator of cell survival and ischemic injury in the heart. *Am. J. Physiol. Heart Circ. Physiol.* **296**, H1–H12 [CrossRef Medline](#)
- Shishido, T., Nozaki, N., Yamaguchi, S., Shibata, Y., Nitobe, J., Miyamoto, T., Takahashi, H., Arimoto, T., Maeda, K., Yamakawa, M., Takeuchi, O., Akira, S., Takeishi, Y., and Kubota, I. (2003) Toll-like receptor-2 modulates ventricular remodeling after myocardial infarction. *Circulation* **108**, 2905–2910 [CrossRef Medline](#)
- Boehm, O., Knuefermann, P., Plueck, J., Schwederski, M., Ehrentraut, H., Kebir, S., Lohner, R., Velten, M., Morath, S., Koch, A., Zacharowski, K., Grohe, C., Hoeft, A., Baumgarten, G., and Meyer, R. (2013) TLR2 stimulation induces cardiac inflammation but not cardiac depression *in vivo*. *J. Inflamm.* **10**, 33 [CrossRef Medline](#)
- Ma, Y., Zhang, X., Bao, H., Mi, S., Cai, W., Yan, H., Wang, Q., Wang, Z., Yan, J., Fan, G., Lindsey, M. L., and Hu, Z. (2012) Toll-like receptor (TLR) 2 and TLR4 differentially regulate doxorubicin induced cardiomyopathy in mice. *PLoS One* **7**, e40763 [CrossRef Medline](#)
- Mullick, A. E., Tobias, P. S., and Curtiss, L. K. (2005) Modulation of atherosclerosis in mice by Toll-like receptor 2. *J. Clin. Invest.* **115**, 3149–3156 [CrossRef Medline](#)
- Bualeong, T., Kebir, S., Hof, D., Goelz, L., Graewe, M., Ehrentraut, S. F., Knuefermann, P., Baumgarten, G., Meyer, R., and Ehrentraut, H. (2016) Tlr2 deficiency does not limit the development of left ventricular hypertrophy in a model of transverse aortic constriction induced pressure overload. *J. Negat. Results Biomed.* **15**, 9 [CrossRef Medline](#)
- Shechter, R., London, A., Kuperman, Y., Ronen, A., Rolls, A., Chen, A., and Schwartz, M. (2013) Hypothalamic neuronal Toll-like receptor 2 protects against age-induced obesity. *Sci. Rep.* **3**, 1254 [CrossRef Medline](#)
- Albert, E. J., and Marshall, J. S. (2008) Aging in the absence of TLR2 is associated with reduced IFN- $\gamma$  responses in the large intestine and increased severity of induced colitis. *J. Leukocyte Biol.* **83**, 833–842 [CrossRef Medline](#)
- Shaw, A. C., Panda, A., Joshi, S. R., Qian, F., Allore, H. G., and Montgomery, R. R. (2011) Dysregulation of human Toll-like receptor function in aging. *Ageing Res. Rev.* **10**, 346–353 [CrossRef Medline](#)
- Arbibe, L., Mira, J. P., Teusch, N., Kline, L., Guha, M., Mackman, N., Godowski, P. J., Ulevitch, R. J., and Knaus, U. G. (2000) Toll-like receptor 2-mediated NF- $\kappa$ B activation requires a Rac1-dependent pathway. *Nat. Immunol.* **1**, 533–540 [CrossRef Medline](#)

26. Marmiroli, S., Bavelloni, A., Faenza, I., Sirri, A., Ognibene, A., Cenni, V., Tsukada, J., Koyama, Y., Ruzzene, M., Ferri, A., Auron, P. E., Toker, A., and Maraldi, N. M. (1998) Phosphatidylinositol 3-kinase is recruited to a specific site in the activated IL-1 receptor I. *FEBS Lett.* **438**, 49–54 [CrossRef](#) [Medline](#)
27. Ha, T., Liu, L., Kelley, J., Kao, R., Williams, D., and Li, C. (2011) Toll-like receptors: New players in myocardial ischemia/reperfusion injury. *Antioxid. Redox Signal.* **15**, 1875–1893 [CrossRef](#) [Medline](#)
28. Sussman, M. (2007) “AKT”ing lessons for stem cells: Regulation of cardiac myocyte and progenitor cell proliferation. *Trends Cardiovasc. Med.* **17**, 235–240 [CrossRef](#) [Medline](#)
29. Ronnebaum, S. M., and Patterson, C. (2010) The FoxO family in cardiac function and dysfunction. *Annu. Rev. Physiol.* **72**, 81–94 [CrossRef](#) [Medline](#)
30. Toth, M. J., Ward, K., van der Velden, J., Miller, M. S., Vanburen, P., Lewinter, M. M., and Ades, P. A. (2011) Chronic heart failure reduces Akt phosphorylation in human skeletal muscle: Relationship to muscle size and function. *J. Appl. Physiol.* **110**, 892–900 [CrossRef](#) [Medline](#)
31. Battiprolu, P. K., Hojaye, B., Jiang, N., Wang, Z. V., Luo, X., Iglewski, M., Shelton, J. M., Gerard, R. D., Rothermel, B. A., Gillette, T. G., Lavandro, S., and Hill, J. A. (2012) Metabolic stress-induced activation of FoxO1 triggers diabetic cardiomyopathy in mice. *J. Clin. Invest.* **122**, 1109–1118 [CrossRef](#) [Medline](#)
32. Galasso, G., De Rosa, R., Piscione, F., Iaccarino, G., Vosa, C., Sorriento, D., Piccolo, R., Luciano, R., Walsh, K., and Chiariello, M. (2010) Myocardial expression of Foxo3a-atrogin-1 pathway in human heart failure. *Eur. Heart J.* **31**, 733–733
33. Lin, J., Lopez, E. F., Jin, Y., Van Remmen, H., Bauch, T., Han, H. C., and Lindsey, M. L. (2008) Age-related cardiac muscle sarcopenia: Combining experimental and mathematical modeling to identify mechanisms. *Exp. Gerontol.* **43**, 296–306 [CrossRef](#) [Medline](#)
34. Ramos, G. C., van den Berg, A., Nunes-Silva, V., Weirather, J., Peters, L., Burkard, M., Friedrich, M., Pinnecker, J., Abesser, M., Heinze, K. G., Schuh, K., Beyersdorf, N., Kerkau, T., Demengeot, J., Frantz, S., and Hofmann, U. (2017) Myocardial aging as a T-cell-mediated phenomenon. *Proc. Natl. Acad. Sci. U.S.A.* **114**, E2420–E2429 [CrossRef](#) [Medline](#)
35. Lee, C. K., Allison, D. B., Brand, J., Weindruch, R., and Prolla, T. A. (2002) Transcriptional profiles associated with aging and middle age-onset caloric restriction in mouse hearts. *Proc. Natl. Acad. Sci. U.S.A.* **99**, 14988–14993 [CrossRef](#) [Medline](#)
36. Lu, L., Guo, J. B., Hua, Y., Huang, K., Magaye, R., Cornell, J., Kelly, D. J., Reid, C., Liew, D., Zhou, Y. C., Chen, A. H., Xiao, W., Fu, Q., and Wang, B. H. (2017) Cardiac fibrosis in the ageing heart: Contributors and mechanisms. *Clin. Exp. Pharmacol. Physiol.* **44**, Suppl. 1, 55–63 [CrossRef](#) [Medline](#)
37. Connell, P. S., Han, R. I., and Grande-Allen, K. J. (2012) Differentiating the aging of the mitral valve from human and canine myxomatous degeneration. *J. Vet. Cardiol.* **14**, 31–45 [CrossRef](#) [Medline](#)
38. Kajstura, J., Cheng, W., Sarangarajan, R., Li, P., Li, B. S., Nitahara, J. A., Chappnick, S., Reiss, K., Olivetti, G., and Anversa, P. (1996) Necrotic and apoptotic myocyte cell death in the aging heart of Fischer 344 rats. *Am. J. Physiol. Heart Circ. Physiol.* **271**, H1215–H1228 [CrossRef](#) [Medline](#)
39. Elmore, S. (2007) Apoptosis: A review of programmed cell death. *Toxicol. Pathol.* **35**, 495–516 [CrossRef](#) [Medline](#)
40. Molnár, A., Tóth, A., Bagi, Z., Papp, Z., Edes, I., Vaszily, M., Galajda, Z., Papp, J. G., Varró, A., Szüts, V., Lacza, Z., Gerö, D., and Szabó, C. (2006) Activation of the poly(ADP-ribose) polymerase pathway in human heart failure. *Mol. Med.* **12**, 143–152 [Medline](#)
41. Mishra, S., Tamta, A. K., Sarikhani, M., Desingu, P. A., Kizkekra, S. M., Pandit, A. S., Kumar, S., Khan, D., Raghavan, S. C., and Sundaresan, N. R. (2018) Subcutaneous Ehrlich ascites carcinoma mice model for studying cancer-induced cardiomyopathy. *Sci. Rep.* **8**, 5599 [CrossRef](#) [Medline](#)
42. Pinto, A. R., Godwin, J. W., Chandran, A., Hersey, L., Ilinykh, A., Debuque, R., Wang, L., and Rosenthal, N. A. (2014) Age-related changes in tissue macrophages precede cardiac functional impairment. *Aging* **6**, 399–413 [CrossRef](#) [Medline](#)
43. Hattori, Y., and Kasai, K. (1997) Induction of mRNAs for ICAM-1, VCAM-1, and ELAM-1 in cultured rat cardiac myocytes and myocardium *in vivo*. *Biochem. Mol. Biol. Int.* **41**, 979–986 [Medline](#)
44. Salvador, A. M., Nevers, T., Velázquez, F., Aronovitz, M., Wang, B., Abadía Molina, A., Jaffe, I. Z., Karas, R. H., Blanton, R. M., and Alcaide, P. (2016) Intercellular adhesion molecule 1 (ICAM-1) regulates cardiac remodeling and function in pressure overload induced heart failure. *J. Am. Heart Assoc.* **5**, e003126 [Medline](#)
45. Richter, V., Rassoul, F., Purschwitz, K., Hentschel, B., Reuter, W., and Kuntze, T. (2003) Circulating vascular cell adhesion molecules VCAM-1, ICAM-1, and E-selectin in dependence on aging. *Gerontology* **49**, 293–300 [CrossRef](#) [Medline](#)
46. Sussman, M. A., Völkers, M., Fischer, K., Bailey, B., Cottage, C. T., Din, S., Gude, N., Avitabile, D., Alvarez, R., Sundararaman, B., Quijada, P., Mason, M., Konstantin, M. H., Malhowski, A., Cheng, Z., Khan, M., and McGregor, M. (2011) Myocardial AKT: the omnipresent nexus. *Physiol. Rev.* **91**, 1023–1070 [CrossRef](#) [Medline](#)
47. Van Der Heide, L. P., Hoekman, M. F., and Smidt, M. P. (2004) The ins and outs of FoxO shuttling: mechanisms of FoxO translocation and transcriptional regulation. *Biochem. J.* **380**, 297–309 [CrossRef](#) [Medline](#)
48. Milan, G., Romanello, V., Pescatore, F., Armani, A., Paik, J. H., Frasson, L., Seydel, A., Zhao, J., Abraham, R., Goldberg, A. L., Blaauw, B., DePinho, R. A., and Sandri, M. (2015) Regulation of autophagy and the ubiquitin-proteasome system by the FoxO transcriptional network during muscle atrophy. *Nat. Commun.* **6**, 6670 [CrossRef](#) [Medline](#)
49. Herman, A. C., Monlish, D. A., Romine, M. P., Bhatt, S. T., Zippel, S., and Schuettelpelz, L. G. (2016) Systemic TLR2 agonist exposure regulates hematopoietic stem cells via cell-autonomous and cell-non-autonomous mechanisms. *Blood Cancer J.* **6**, e437 [CrossRef](#) [Medline](#)
50. Park, S. J., Lee, J. Y., Kim, S. J., Choi, S. Y., Yune, T. Y., and Ryu, J. H. (2015) Toll-like receptor-2 deficiency induces schizophrenia-like behaviors in mice. *Sci. Rep.* **5**, 8502 [CrossRef](#) [Medline](#)
51. Lu, C., Liu, L., Chen, Y., Ha, T., Kelley, J., Schweitzer, J., Kalbfleisch, J. H., Kao, R. L., Williams, D. L., and Li, C. (2011) TLR2 ligand induces protection against cerebral ischemia/reperfusion injury via activation of phosphoinositide 3-kinase/Akt signaling. *J. Immunol.* **187**, 1458–1466 [CrossRef](#) [Medline](#)
52. Timmerman, K. L., and Rasmussen, B. B. (2011) Does a reduction in anabolic signaling contribute to muscle wasting in chronic heart failure? *J. Appl. Physiol.* **110**, 869–870 [CrossRef](#) [Medline](#)
53. Pourrajab, F., Yazdi, M. B., Zarch, M. B., Zarch, M. B., and Hekmatimoghaddam, S. (2015) Cross talk of the first-line defense TLRs with PI3K/Akt pathway, in preconditioning therapeutic approach. *Mol. Cell. Ther.* **3**, 4 [CrossRef](#) [Medline](#)
54. Sandor, F., Latz, E., Re, F., Mandell, L., Repik, G., Golenbock, D. T., Espevik, T., Kurt-Jones, E. A., and Finberg, R. W. (2003) Importance of extra- and intracellular domains of TLR1 and TLR2 in NFκB signaling. *J. Cell Biol.* **162**, 1099–1110 [CrossRef](#) [Medline](#)
55. Gautam, J. K., Ashish, Comeau, L. D., Krueger, J. K., and Smith, M. F., Jr. (2006) Structural and functional evidence for the role of the TLR2 DD loop in TLR1/TLR2 heterodimerization and signaling. *J. Biol. Chem.* **281**, 30132–30142 [CrossRef](#) [Medline](#)
56. Farhat, K., Riekenberg, S., Heine, H., Debarry, J., Lang, R., Mages, J., Buwitt-Beckmann, U., Röschmann, K., Jung, G., Wiesmüller, K. H., and Ulmer, A. J. (2008) Heterodimerization of TLR2 with TLR1 or TLR6 expands the ligand spectrum but does not lead to differential signaling. *J. Leukoc. Biol.* **83**, 692–701 [CrossRef](#) [Medline](#)
57. Cuevas, C. D., and Ross, S. R. (2014) Toll-like receptor 2-mediated innate immune responses against Junin virus in mice lead to antiviral adaptive immune responses during systemic infection and do not affect viral replication in the brain. *J. Virol.* **88**, 7703–7714 [CrossRef](#) [Medline](#)
58. Massari, P., Visintin, A., Gunawardana, J., Halmen, K. A., King, C. A., Golenbock, D. T., and Wetzler, L. M. (2006) Meningococcal porin PorB binds to TLR2 and requires TLR1 for signaling. *J. Immunol.* **176**, 2373–2380 [CrossRef](#) [Medline](#)
59. Oliveira-Nascimento, L., Massari, P., and Wetzler, L. M. (2012) The role of TLR2 in infection and immunity. *Front. Immunol.* **3**, 79 [Medline](#)

60. Chen, Q., Wang, Z. Y., Chen, L. Y., and Hu, H. Y. (2017) Roles of high mobility group box 1 in cardiovascular calcification. *Cell. Physiol. Biochem.* **42**, 427–440 [CrossRef Medline](#)
61. Menon, R., Mesiano, S., and Taylor, R. N. (2017) Programmed fetal membrane senescence and exosome-mediated signaling: A mechanism associated with timing of human parturition. *Front. Endocrinol. (Lausanne)* **8**, 196 [CrossRef Medline](#)
62. Sloane, J. A., Blitz, D., Margolin, Z., and Vartanian, T. (2010) A clear and present danger: Endogenous ligands of Toll-like receptors. *Neuromolecular Med.* **12**, 149–163 [CrossRef Medline](#)
63. Tamura, Y., Torigoe, T., Kutomi, G., Hirata, K., and Sato, N. (2012) New paradigm for intrinsic function of heat shock proteins as endogenous ligands in inflammation and innate immunity. *Curr. Mol. Med.* **12**, 1198–1206 [CrossRef Medline](#)
64. Weinberger, T., and Schulz, C. (2015) Myocardial infarction: A critical role of macrophages in cardiac remodeling. *Front. Physiol.* **6**, 107 [Medline](#)
65. Hulsmans, M., Clauss, S., Xiao, L., Aguirre, A. D., King, K. R., Hanley, A., Hucker, W. J., Wülfers, E. M., Seemann, G., Courties, G., Iwamoto, Y., Sun, Y., Savol, A. J., Sager, H. B., Lavine, K. J., et al. (2017) Macrophages facilitate electrical conduction in the heart. *Cell* **169**, 510–522.e520 [CrossRef Medline](#)
66. Chen, B., and Frangogiannis, N. G. (2016) Macrophages in the remodeling failing heart. *Circ. Res.* **119**, 776–778 [CrossRef Medline](#)
67. Favre, J., Musette, P., Douin-Echinard, V., Laude, K., Henry, J. P., Arnal, J. F., Thuillez, C., and Richard, V. (2007) Toll-like receptors 2-deficient mice are protected against postischemic coronary endothelial dysfunction. *Arterioscler. Thromb. Vasc. Biol.* **27**, 1064–1071 [CrossRef Medline](#)
68. van Duin, D., Mohanty, S., Thomas, V., Ginter, S., Montgomery, R. R., Fikrig, E., Allore, H. G., Medzhitov, R., and Shaw, A. C. (2007) Age-associated defect in human TLR-1/2 function. *J. Immunol.* **178**, 970–975 [CrossRef Medline](#)
69. Agius, E., Lacy, K. E., Vukmanovic-Stejic, M., Jagger, A. L., Papageorgiou, A. P., Hall, S., Reed, J. R., Curnow, S. J., Fuentes-Duculan, J., Buckley, C. D., Salmon, M., Taams, L. S., Krueger, J., Greenwood, J., Klein, N., et al. (2009) Decreased TNF- $\alpha$  synthesis by macrophages restricts cutaneous immunosurveillance by memory CD4+ T cells during aging. *J. Exp. Med.* **206**, 1929–1940 [CrossRef Medline](#)
70. Kong, K. F., Delroux, K., Wang, X., Qian, F., Arjona, A., Malawista, S. E., Fikrig, E., and Montgomery, R. R. (2008) Dysregulation of TLR3 impairs the innate immune response to West Nile virus in the elderly. *J. Immunol.* **182**, 7613–7623 [Medline](#)
71. Agrawal, A., Agrawal, S., Cao, J. N., Su, H., Osann, K., and Gupta, S. (2007) Altered innate immune functioning of dendritic cells in elderly humans: A role of phosphoinositide 3-kinase-signaling pathway. *J. Immunol.* **178**, 6912–6922 [CrossRef Medline](#)
72. Arbour, N. C., Lorenz, E., Schutte, B. C., Zabner, J., Kline, J. N., Jones, M., Frees, K., Watt, J. L., and Schwartz, D. A. (2000) TLR4 mutations are associated with endotoxin hyporesponsiveness in humans. *Nat. Genet.* **25**, 187–191 [CrossRef Medline](#)
73. Ferwerda, B., McCall, M. B., Alonso, S., Giamarellos-Bourboulis, E. J., Mouktaroudi, M., Izagirre, N., Syafruddin, D., Kibiki, G., Cristea, T., Hijmans, A., Hamann, L., Israel, S., ElGhazali, G., Troye-Blomberg, M., Kumpf, O., et al. (2007) TLR4 polymorphisms, infectious diseases, and evolutionary pressure during migration of modern humans. *Proc. Natl. Acad. Sci. U.S.A.* **104**, 16645–16650 [CrossRef Medline](#)
74. Calvano, J. E., Bowers, D. J., Coyle, S. M., Macor, M., Reddell, M. T., Kumar, A., Calvano, S. E., and Lowry, S. F. (2006) Response to systemic endotoxemia among humans bearing polymorphisms of the Toll-like receptor 4 (hTLR4). *Clin. Immunol.* **121**, 186–190 [CrossRef Medline](#)
75. Erridge, C., Stewart, J., and Poxton, I. R. (2003) Monocytes heterozygous for the Asp299Gly and Thr399Ile mutations in the Toll-like receptor 4 gene show no deficit in lipopolysaccharide signalling. *J. Exp. Med.* **197**, 1787–1791 [CrossRef Medline](#)
76. Schippers, E. F., van 't Veer, C., van Voorden, S., Martina, C. A., le Cessie, S., and van Dissel, J. T. (2004) TNF- $\alpha$  promoter, Nod2 and toll-like receptor-4 polymorphisms and the *in vivo* and *ex vivo* response to endotoxin. *Cytokine* **26**, 16–24 [CrossRef Medline](#)
77. Balistreri, C. R., Candore, G., Colonna-Romano, G., Lio, D., Caruso, M., Hoffmann, E., Franceschi, C., and Caruso, C. (2004) Role of Toll-like receptor 4 in acute myocardial infarction and longevity. *JAMA* **292**, 2339–2340 [CrossRef Medline](#)
78. Jain, A., Ravi, V., Muhamed, J., Chatterjee, K., and Sundaresan, N. R. (2017) A simplified protocol for culture of murine neonatal cardiomyocytes on nanoscale keratin coated surfaces. *Int. J. Cardiol.* **232**, 160–170 [CrossRef Medline](#)
79. Sundaresan, N. R., Vasudevan, P., Zhong, L., Kim, G., Samant, S., Parekh, V., Pillai, V. B., Ravindra, P. V., Gupta, M., Jeevanandam, V., Cunningham, J. M., Deng, C. X., Lombard, D. B., Mostoslavsky, R., and Gupta, M. P. (2012) The sirtuin SIRT6 blocks IGF-Akt signaling and development of cardiac hypertrophy by targeting c-Jun. *Nat. Med.* **18**, 1643–1650 [CrossRef Medline](#)
80. Ackers-Johnson, M., Li, P. Y., Holmes, A. P., O'Brien, S. M., Pavlovic, D., and Foo, R. S. (2016) A simplified, Langendorff-free method for concomitant isolation of viable cardiac myocytes and nonmyocytes from the adult mouse heart. *Circ. Res.* **119**, 909–920 [CrossRef Medline](#)
81. Yadav, S., Pathak, S., Sarikhani, M., Majumdar, S., Ray, S., Chandrasekar, B. S., Adiga, V., Sundaresan, N. R., and Nandi, D. (2018) Nitric oxide synthase 2 enhances the survival of mice during *Salmonella typhimurium* infection-induced sepsis by increasing reactive oxygen species, inflammatory cytokines and recruitment of neutrophils to the peritoneal cavity. *Free. Radic. Biol. Med.* **116**, 73–87 [CrossRef Medline](#)